

Electronic Supporting Information

White-light emission from a pyrimidine-carbazole conjugate with tunable phosphorescence-fluorescence dual emission and multicolor emission switching

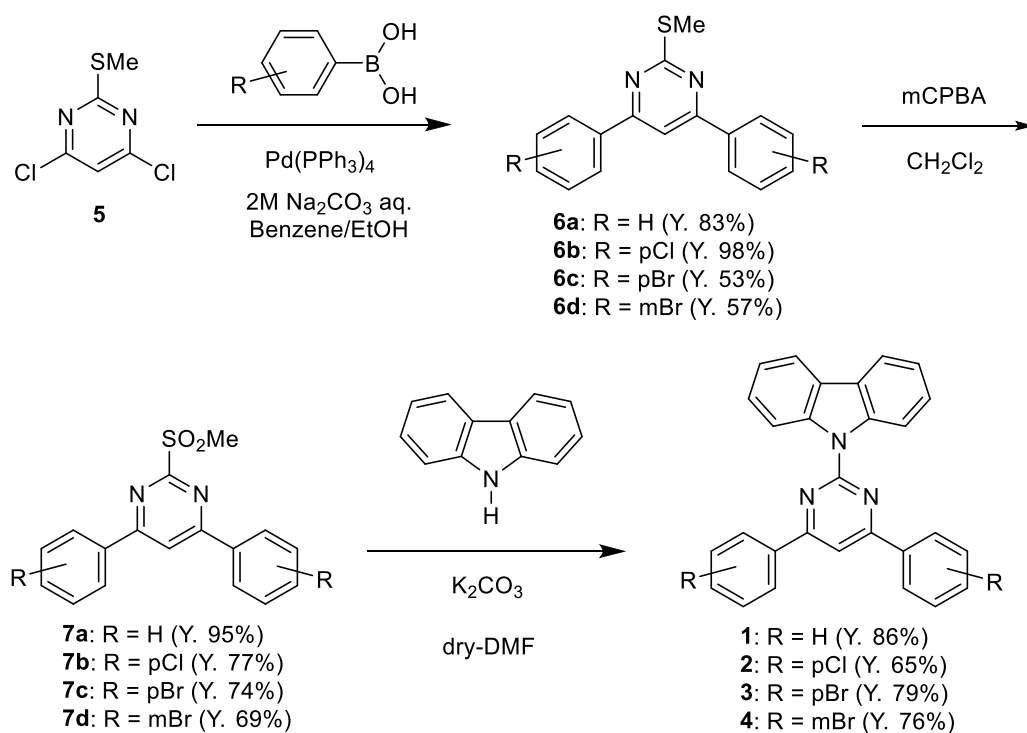
Tsutomu Ishii,^{*a} Honoka Tanaka,^{ab} In Seob Park,^c Takuma Yasuda,^c Shin-ichiro Kato,^d Mitsunori Ito,^e Hidetaka Hiyoshi^e and Taisuke Matsumoto^f

Table of Contents

Experimental section	2-9
Absorption and fluorescence spectra in solution: Figs. S1 and S2	10
Excitation and diffuse reflection spectra in the solid state: Fig. S3	11
Steady-state fluorescence spectra in the solid state: Figs. S4-S11	11-16
Fluorescence and phosphorescence lifetime: Figs. S12 and S13	17
Spectral data of absorption, fluorescence, and phosphorescence spectra: Tables S1 and S2	18-19
Powder X-ray diffraction measurement: Figs. S14-S17	20-22
Differential scanning calorimetry: Figs. S18 and S19, and Table S3	23-24
Single crystal X-ray diffraction analysis: Figs. S20-S24, and Tables S4 and S5	25-34
Chemical structure of three possible conformations in 4 : Figs. S25	35
Computer simulation analysis: Fig. S26 and Tables S6-S10	35-41
¹ H and ¹³ C NMR spectra of new compounds; Figs. S27-S50	42-53

Experimental Section

General. All melting points are uncorrected. IR spectra were recorded on a JASCO FT/IR-470 plus Fourier transform infrared spectrometer, and measured on KBr pellets. ^1H and ^{13}C NMR spectra were determined in CDCl_3 or $\text{CDCl}_2\text{CDCl}_2$ with a JEOL ECX 500 spectrometer. Residual solvent protons were used as internal standard and chemical shifts (δ) are given relative to tetramethylsilane (TMS). The coupling constants (J) are reported in hertz (Hz). Elemental analysis was performed at the Elemental Analytical Center, Kyushu University. Fast atom bombardment mass spectrometry (FAB-MS) spectra were recorded with a JEOL JMS-70 mass spectrometer with *m*-nitrobenzyl alcohol (NBA) as a matrix. Gel permeation chromatography (GPC) was performed with a Japan Analytical Industry LC-908 using JAIGEL-1H column (20×600 mm) and JAIGEL-2H column (20×600 mm) eluting with chloroform (3.0 mL/min). Analytical TLC was carried out on silica gel coated on aluminum foil (Merck 60 F254). Column chromatography was carried out on silica gel (WAKO C300). All chemicals and solvents were commercial available and were used without further purification except for carbazole, which was purified by recrystallization from acetone.



2-(Methylsulfanyl)-4,6-diphenylpyrimidine (6a). To a mixture of dichloropyrimidine **5** (980 mg, 5.0 mmol) and phenylboronic acid (1.34 g, 11 mmol) tetrakis(triphenylphosphine)palladium(0) (289 mg, 0.25 mmol) were added in deaerated benzene (100 mL), ethanol (25 mL), and aqueous 2 M sodium carbonate (50 mL). Then the mixture was heated at 85 °C under an argon atmosphere for 15 h. After the reaction mixture was poured into water, it was extracted with dichloromethane. The combined organic layer was washed with brine and water, dried over anhydrous magnesium sulfate, and evaporated in vacuo to dryness. The residue was purified by silica gel column chromatography (WAKO C300) eluting with hexane/dichloromethane (3:1, v/v) to give **6a** in 83% (1.158 g, 4.160 mmol). An analytical sample was obtained by recrystallization from hexane/dichloromethane as a white powder: mp 153–154 °C; IR (KBr, cm^{-1}) 3054, 2914, 1569, 1559, 1521, 1507, 1496, 1363, 1249, 1077, 847, 782, 754, 696, 656; ^1H NMR (CDCl_3 , 500 MHz) δ 2.73 (s, 3 H, CH_3), 7.50–7.54 (m, 6 H, ArH), 7.78 (s, 1 H, ArH), 8.14–8.18 (m, 4 H, ArH); ^{13}C NMR (CDCl_3 , 126 MHz) δ 14.36, 107.88, 127.23, 128.85, 130.91, 136.89, 164.65, 172.75; FAB-MS (positive, NBA) m/z 278 (M^+). Anal. Calcd for $\text{C}_{17}\text{H}_{14}\text{N}_2\text{S}$ (278.37): C, 73.35; H, 5.07; N, 10.06. Found: C, 73.17; H, 5.02; N, 10.06.

4,6-Bis(4-chlorophenyl)-2-(methylsulfanyl)pyrimidine (6b). According to the method for the preparation of **6a**, **6b** was obtained in 98% yield (1.03 g, 2.98 mmol) from dichloropyrimidine **5** (585 mg, 3.0 mmol), boronic acid (1.03 g, 6.6 mmol) tetrakis(triphenylphosphine)palladium(0) (347 mg, 0.3 mmol), deaerated benzene (60 mL), ethanol (15 mL), and aqueous 2 M sodium carbonate (30 mL). The reaction mixture was purified by silica gel column chromatography (WAKO C300) eluting with hexane/dichloromethane (4:1, v/v). White solid (hexane/dichloromethane); mp 148–149 °C; IR (KBr, cm^{-1}) 3060, 2996, 2924, 2854, 1582, 1567, 1515, 1491, 1364, 1320, 1283, 1241, 1092, 1011, 823, 762; ^1H NMR (CDCl_3 , 500 MHz) δ 2.71 (s, 3 H, CH_3), 7.49 (d, $J = 8.6$ Hz, 4 H, ArH), 7.70 (s, 1 H, ArH), 8.10 (d, $J = 8.6$ Hz, 4 H, ArH); ^{13}C NMR (CDCl_3 , 126 MHz) δ 14.38, 107.21, 128.51, 129.14, 135.09, 137.29, 163.56, 173.08; FAB-MS (positive, NBA) m/z 347 [$(\text{M}+1)^+$]. Anal. Calcd for $\text{C}_{17}\text{H}_{12}\text{Cl}_2\text{N}_2\text{S}$ (347.26): C, 58.80; H, 3.48; N, 8.07. Found: C, 58.72; H, 3.38; N, 8.12.

4,6-Bis(4-bromophenyl)-2-(methylsulfanyl)pyrimidine (6c). According to the method for the preparation of **6a**, **6c** was obtained in 53% (462 mg, 1.059 mmol) from dichloropyrimidine **5** (390 mg, 2.0 mmol), boronic acid (884 mg, 4.4 mmol) tetrakis(triphenylphosphine)palladium(0) (231 mg, 0.2 mmol), deaerated benzene (40 mL), ethanol (10 mL), and aqueous 2 M sodium carbonate (20 mL). The reaction mixture was purified by silica gel column chromatography (WAKO C300) eluting with hexane/dichloromethane (3:1, v/v). White solid (chloroform); mp 148–149 °C; IR (KBr, cm^{-1}) 3058, 2990, 2922, 1589, 1577, 1556, 1510, 1486, 1306, 1280, 1241, 1065, 1009, 819; ^1H NMR (CDCl_3 , 500 MHz) δ 2.70 (s, 3 H, CH_3), 7.65 (d, $J = 8.6$ Hz, 4 H, ArH), 7.70 (s, 1 H, ArH), 8.03 (d, $J = 8.6$ Hz, 4 H, ArH); ^{13}C NMR (CDCl_3 , 126 MHz) δ 14.38, 107.17, 125.78, 128.76, 132.13, 135.60, 163.72, 173.19; FAB-MS (positive, NBA) m/z 435, 437, 439 [($\text{M}+1$) $^+$]. Anal. Calcd for $\text{C}_{17}\text{H}_{12}\text{Br}_2\text{N}_2\text{S}$ (436.16): C, 46.81; H, 2.77; N, 6.42. Found: C, 46.66; H, 2.71; N, 6.37.

4,6-Bis(3-bromophenyl)-2-(methylsulfanyl)pyrimidine (6d). According to the method for the preparation of **6a**, **6d** was obtained in 57% (751 mg, 1.722 mmol) from dichloropyrimidine **5** (585 mg, 3.0 mmol), boronic acid (1.33 g, 6.6 mmol) tetrakis(triphenylphosphine)palladium(0) (347 mg, 0.3 mmol), deaerated benzene (60 mL), ethanol (15 mL), and aqueous 2 M sodium carbonate (30 mL). The reaction mixture was purified by silica gel column chromatography (WAKO C300) eluting with hexane/dichloromethane (3:1, v/v). White solid (hexane/dichloromethane); mp 142–143 °C; IR (KBr, cm^{-1}) 3078, 3061, 2922, 1574, 1561, 1516, 1289, 1244, 768, 710, 685; ^1H NMR (CDCl_3 , 500 MHz) δ 2.72 (s, 3 H, CH_3), 7.40 (t, $J = 8.0$ Hz, 2 H, ArH), 7.66 (d, $J = 8.0$ Hz, 2 H, ArH), 7.69 (s, 1 H, ArH), 8.08 (d, $J = 8.0$ Hz, 2 H, ArH), 8.30 (s, 2 H, ArH); ^{13}C NMR (CDCl_3 , 126 MHz) δ 14.42, 107.84, 123.19, 125.84, 130.30, 130.43, 133.98, 138.71, 163.42, 173.32; FAB-MS (positive, NBA) m/z 435, 437, 439 [($\text{M}+1$) $^+$]. Anal. Calcd for $\text{C}_{17}\text{H}_{12}\text{Br}_2\text{N}_2\text{S}$ (436.16): C, 46.81; H, 2.77; N, 6.42. Found: C, 46.78; H, 2.78; N, 6.18.

2-Methanesulfonyl-4,6-diphenylpyrimidine (7a). To a solution of **6a** (557 mg, 2.0 mmol) in dichloromethane (150 mL, dried over 4A molecular sieves) was added mCPBA (75 wt-% including water, 2.26 g, 9.8 mmol) at 0 °C. The mixture was stirred at room temperature for 2 h. After the reaction mixture was

poured into 10 wt-% aqueous solution of sodium hydrogen sulfite, it was extracted with dichloromethane. The organic layer was washed with 10 wt-% aqueous solution of sodium hydrogen sulfite, 1 M aqueous solution of sodium hydrogen carbonate, and water, dried over anhydrous magnesium sulfate, and evaporated in vacuo to dryness. The residue was purified by silica gel column chromatography (WAKO C300) eluting with chloroform to give **7a** in 95% (590 mg, 1.90 mmol) as a white solid: mp 215–216 °C; IR (KBr, cm^{-1}) 3060, 3040, 3027, 2942, 1585, 1575, 1509, 1496, 1427, 1364, 1315, 1301 (ν_{SO_2}), 1248, 1139 (ν_{SO_2}), 957, 787, 754, 689, 626; $^1\text{H NMR}$ (CDCl_3 , 500 MHz) δ 3.50 (s, 3 H, CH_3), 7.54–7.63 (m, 6 H, ArH), 8.23 (d, $J = 8.6$ Hz, 4 H, ArH), 8.27 (s, 1 H, ArH); $^{13}\text{C NMR}$ (CDCl_3 , 126 MHz) δ 39.10, 114.12, 127.59, 129.22, 132.16, 135.10, 166.50, 166.56; FAB-MS (positive, NBA) m/z 311 $[(\text{M}+1)^+]$. Anal. Calcd for $\text{C}_{17}\text{H}_{14}\text{N}_2\text{O}_2\text{S}$ (310.37): C, 65.79; H, 4.55; N, 9.03. Found: C, 65.75; H, 4.60; N, 8.91.

4,6-Bis(4-chlorophenyl)-2-methanesulfonylpyrimidine (7b). According to the method for the preparation of **7a**, **7b** was obtained in 77% (784 mg, 2.07 mmol) from **6b** (934 mg, 2.7 mmol), mCPBA (3.04 g, 13.2 mmol), and dichloromethane (203 mL). The reaction mixture was purified by silica gel column chromatography (WAKO C300) eluting with chloroform to give pure **7b** as a white solid: mp 250–251 °C; IR (KBr, cm^{-1}) 3095, 3066, 3032, 3010, 2930, 1583, 1569, 1505, 1494, 1434, 1367, 1308 (ν_{SO_2}), 1291, 1251, 1138 (ν_{SO_2}), 1091, 1011, 956, 837, 760; $^1\text{H NMR}$ (CDCl_3 , 500 MHz) δ 3.49 (s, 3 H, CH_3), 7.55 (d, $J = 8.6$ Hz, 4 H, ArH), 8.18 (d, $J = 8.6$ Hz, 4 H, ArH), 8.19 (s, 1 H, ArH); $^{13}\text{C NMR}$ (CDCl_3 , 126 MHz) δ 39.10, 113.58, 128.87, 129.58, 133.31, 138.80, 165.49, 166.66; FAB-MS (positive, NBA) m/z 379 $[(\text{M}+1)^+]$. Anal. Calcd for $\text{C}_{17}\text{H}_{12}\text{Cl}_2\text{N}_2\text{O}_2\text{S}$ (379.26): C, 53.84; H, 3.19; N, 7.39. Found: C, 53.84; H, 3.13; N, 7.44.

4,6-Bis(4-bromophenyl)-2-methanesulfonylpyrimidine (7c). According to the method for the preparation of **7a**, **7c** was obtained in 74% (349 mg, 0.746 mmol) from **6c** (442 mg, 1.01 mmol), mCPBA (1.13 g, 4.9 mmol), and dichloromethane (75 mL). The reaction mixture was suspended in dichloromethane and filtrated to give **7c**. An analytical sample was obtained by recrystallization from DMF to give a white solid; mp 252–253 °C; IR (KBr, cm^{-1}) 3096, 3059, 3032, 3009, 2929, 1579, 1566, 1501, 1490, 1434, 1365, 1306 (ν_{SO_2}), 1290, 1250,

1138 (ν_{SO_2}), 1071, 1007, 834, 822, 758; $^1\text{H NMR}$ ($\text{CDCl}_2\text{CDCl}_2$, 500 MHz) δ 3.49 (s, 3 H, CH_3), 7.74 (d, $J = 8.6$ Hz, 4 H, ArH), 8.09 (d, $J = 8.6$ Hz 4 H, ArH), 8.19 (s, 1 H, ArH) $^{13}\text{C NMR}$ ($\text{CDCl}_2\text{CDCl}_2$, 126 MHz) δ 39.64, 114.19, 127.70, 129.38, 132.95, 134.02, 166.02, 166.68; FAB-MS (positive, NBA) m/z 467, 469, 471 $[(M+1)^+]$. Anal. Calcd for $\text{C}_{17}\text{H}_{12}\text{Br}_2\text{N}_2\text{O}_2\text{S}$ (468.16): C, 43.61; H, 2.58; N, 5.98. Found: C, 43.72; H, 2.57; N, 6.01.

4,6-Bis(3-bromophenyl)-2-methanesulfonylpyrimidine (7d). According to the method for the preparation of **7a**, **7d** was obtained in 69% (528 mg, 1.13 mmol) from **6d** (713 mg, 1.64 mmol), mCPBA (1.84 g, 8.0 mmol), and dichloromethane (123 mL). The reaction mixture was suspended in dichloromethane and filtrated to give pure **7d**. An analytical sample was obtained by recrystallization from hexane/chloroform to give a white solid: mp 185–186 °C; IR (KBr, cm^{-1}) 3089, 3066, 3038, 2926, 1580, 1562, 1507, 1431, 1304 (ν_{SO_2}), 1242, 1139 (ν_{SO_2}), 886, 795, 768, 680; $^1\text{H NMR}$ (CDCl_3 , 500 MHz) δ 3.51 (s, 3 H, CH_3), 7.46 (t, $J = 8.0$ Hz, 2 H, ArH), 7.74 (d, $J = 8.0$ Hz 2 H, ArH), 8.16 (d $J = 8.0$ Hz, 2 H, ArH), 8.19 (s, 1 H, ArH), 8.35 (s, 2 H, ArH); $^{13}\text{C NMR}$ (CDCl_3 , 126 MHz) δ 39.18, 114.35, 123.57, 126.26, 130.55, 130.81, 135.27, 136.86, 165.40, 166.76; FAB-MS (positive, NBA) m/z 467, 469, 471 $[(M+1)^+]$. Anal. Calcd for $\text{C}_{17}\text{H}_{12}\text{Br}_2\text{N}_2\text{O}_2\text{S}$ (468.16): C, 43.61; H, 2.58; N, 5.98. Found: C, 43.42; H, 2.57; N, 5.70.

2-(N-Carbazolyl)-4,6-diphenylpyrimidine (1). A mixture of **7a** (425 mg, 1.37 mmol), carbazole (274 mg, 1.64 mmol), and powdered potassium carbonate (1.00 g, 7.25 mmol) in dry DMF (5 mL) was heated at 70 °C under an argon atmosphere for 12 h. After the reaction mixture was quenched by addition of conc. hydrochloric acid (pH 3~4) at 0 °C, it was extracted with dichloromethane. The organic layer was washed with water sufficiently, dried over anhydrous magnesium sulfate, and evaporated in vacuo to dryness. The residue was purified by silica gel column chromatography (WAKO C300) eluting with hexane/dichloromethane (6:4, v/v) to give **1** in 86% (467 mg, 1.18 mmol). An analytical sample was obtained by GPC eluting with chloroform and recrystallization from hexane/dichloromethane as colorless prisms: mp 215–216 °C; IR (KBr, cm^{-1}) 3138, 3053, 1588, 1573, 1533, 1489, 1438, 1361, 1335, 1306, 1218, 1205, 1186,

1032, 857, 761, 751, 719, 686, 648; ^1H NMR (CDCl_3 , 500 MHz) δ 7.40 (t, $J = 8.1$ Hz, 2 H, ArH), 7.56 (t, $J = 8.1$ Hz, 2 H, ArH), 7.60–7.65 (m, 6 H, ArH), 7.99 (s, 1 H, ArH), 8.12 (d, $J = 8.1$ Hz, 2 H, ArH), 8.32 (d, $J = 8.0$ Hz, 4 H, ArH), 8.99 (d, $J = 8.1$ Hz, 2 H, ArH); ^{13}C NMR (CDCl_3 , 126 MHz) δ 107.64, 116.19, 119.54, 122.04, 125.69, 126.52, 127.41, 129.10, 131.08, 137.24, 139.41, 159.38, 166.08; FAB-MS (positive, NBA) m/z 398 $[(\text{M}+1)^+]$. Anal. Calcd for $\text{C}_{28}\text{H}_{19}\text{N}_3$ (397.47): C, 84.61; H, 4.82; N, 10.57. Found: C, 84.45; H, 4.78; N, 10.45.

2-(N-Carbazolyl)-4,6-bis(4-chlorophenyl)pyrimidine (2). According to the method for the preparation of **1**, **2** was obtained in 65% (244 mg, 0.523 mmol) from **7b** (303 mg, 0.80 mmol), carbazole (161 mg, 0.96 mmol), powdered potassium carbonate (553 mg, 4.0 mmol), and dry DMF (8 mL). The reaction mixture was extracted with chloroform. The crude product was suspended in chloroform and filtrated to give pure **2**. An analytical sample was obtained by recrystallization from hot DMF (70 °C) as colorless needles: mp 295–296 °C; IR (KBr, cm^{-1}) 3141, 3052, 1580, 1567, 1527, 1490, 1441, 1412, 1361, 1335, 1093, 822, 753; ^1H NMR (CDCl_3 , 500 MHz) δ 7.41 (t, $J = 8.1$ Hz, 2 H, ArH), 7.55 (t, $J = 8.1$ Hz, 2 H, ArH), 7.58 (d, $J = 8.6$ Hz 4 H, ArH), 7.88 (s, 1 H, ArH), 8.12 (d, $J = 8.1$ Hz, 2 H, ArH), 8.23 (d, $J = 8.6$ Hz, 4 H, ArH), 8.89 (d, $J = 8.1$ Hz, 2 H, ArH); ^{13}C NMR (CDCl_3 , 126 MHz) δ 107.46, 116.46, 119.90, 122.66, 126.12, 126.96, 128.99, 129.70, 135.88, 137.79, 139.68, 159.68, 165.57; FAB-MS (positive, NBA) m/z 466 $[(\text{M}+1)^+]$. Anal. Calcd for $\text{C}_{28}\text{H}_{17}\text{Cl}_2\text{N}_3$ (466.36): C, 72.11; H, 3.67; N, 9.01. Found: C, 71.74; H, 3.61; N, 9.01.

4,6-Bis(4-bromophenyl)-2-(N-carbazolyl)pyrimidine (3). According to the method for the preparation of **1**, **3** was obtained in 79% (246 mg, 0.443 mmol) from **7c** (263 mg, 0.56 mmol), carbazole (112 mg, 0.67 mmol), powdered potassium carbonate (387 mg, 2.8 mmol), and dry DMF (5.6 mL). After the reaction mixture was quenched by addition of water, the precipitate was collected by filtration and washed with water, methanol, and dichloromethane to give pure **3**. An analytical sample was obtained by recrystallization from hot 1,1,2,2-tetrachloroethane (140 °C) as colorless needles: mp 301–302 °C; IR (KBr, cm^{-1}) 3138, 3049, 1589, 1577, 1563, 1523, 1489, 1440, 1410, 1359, 1334, 1074, 1008, 820, 753; ^1H NMR ($\text{CDCl}_2\text{CDCl}_2$, 500 MHz) δ 7.44 (t, $J =$

8.1 Hz, 2 H, ArH), 7.58 (d, $J = 8.1$ Hz, 2 H, ArH), 7.77 (d, $J = 8.6$ Hz, 4 H, ArH), 7.89 (s, 1 H, ArH), 8.14 (d, $J = 8.1$ Hz, 2 H, ArH), 8.17 (d, $J = 8.6$ Hz, 4 H, ArH), 8.88 (d, $J = 8.1$ Hz, 2 H, ArH); ^{13}C NMR ($\text{CDCl}_2\text{CDCl}_2$, 126 MHz) δ 107.51, 116.26, 120.07, 122.72, 125.90, 126.30, 127.11, 129.24, 132.75, 136.09, 139.43, 159.50, 165.54; FAB-MS (positive, NBA) m/z 554, 556, 558 $[(M+1)^+]$. Anal. Calcd for $\text{C}_{28}\text{H}_{17}\text{Br}_2\text{N}_3$ (555.26): C, 60.57; H, 3.09; N, 7.57. Found: C, 60.18; H, 3.07; N, 7.38.

4,6-Bis(3-bromophenyl)-2-(N-carbazolyl)pyrimidine (4). According to the method for the preparation of **1**, **4** was obtained in 76% (480 mg, 0.865 mmol) from **7d** (528 mg, 1.13 mmol), carbazole (226 mg, 1.35 mmol), powdered potassium carbonate (780 mg, 5.6 mmol), and dry DMF (11.3 mL). After the reaction mixture was quenched by addition of water, the precipitate was collected by filtration and washed with water, methanol, and dichloromethane to give pure **4**. One analytical sample of **4A** (white solid) was obtained by evaporation of chloroform solution, whereas, another analytical sample of **4B** (pale yellow solid) was obtained by recrystallization from hexane/chloroform. Pale yellow solid (hexane/chloroform); mp 190–191 °C; IR (KBr, cm^{-1}) 3124, 3063, 3051, 1574, 1533, 1492, 1451, 1335, 1237, 1224, 1210, 775, 745, 720, 670; ^1H NMR (CDCl_3 , 500 MHz) δ 7.41 (t, $J = 8.0$ Hz, 2 H, ArH), 7.50 (t, $J = 8.0$ Hz, 2 H, ArH), 7.56 (t, $J = 7.5$ Hz, 2 H, ArH), 7.73 (d, $J = 7.5$ Hz, 2 H, ArH), 7.87 (s, 1 H, ArH), 8.12 (d, $J = 8.0$ Hz, 2 H, ArH), 8.24 (d, $J = 7.5$ Hz, 2 H, ArH), 8.42 (s, 2 H, ArH), 8.92 (d, $J = 8.0$ Hz, 2 H, ArH); ^{13}C NMR (CDCl_3 , 126 MHz) δ 107.54, 116.20, 119.64, 122.37, 123.35, 125.87, 126.02, 126.66, 130.47, 130.68, 134.11, 139.06, 139.27, 159.38, 164.93; FAB-MS (positive, NBA) m/z 554, 556, 558 $[(M+1)^+]$. Anal. Calcd for $\text{C}_{28}\text{H}_{17}\text{Br}_2\text{N}_3$ (555.26): C, 60.57; H, 3.09; N, 7.57. Found: C, 60.40; H, 3.06; N, 7.56.

Instrumentation. Steady-state fluorescence spectra and excitation were measured on a JASCO FP-8600 fluorescence spectrophotometer. Phosphorescence spectra were measured on a JASCO FP-8600 fluorescence spectrophotometer with delayed mode: a shutter open-close cycle of 400 ms, an acquisition delay time of 150 ms, and an acquisition period of 30–100 ms. Absorption spectra were measured on a JASCO V-570 spectrophotometer. Diffuse reflection spectra were measured on a JASCO V-670 spectrophotometer

equipped with a JASCO ISV-922 integrating sphere system. Film samples for the fluorescence spectral measurement were prepared by drop casting and subsequent spin-coating (2000 rpm, 30 s) from PMMA dichloromethane solution including 1 wt-% **3** or **4** molecule. Absolute photoluminescence quantum yields were determined on a JASCO FP-8600 fluorescence spectrophotometer equipped with a JASCO ILF-835 integrating sphere system. Fluorescence lifetime measurements were made by using a laser diode (340 nm, pulse width 100 ps, repetition rate 20 kHz) and as the excitation light source and a time-correlated single-photon counting fluorometer (Hamamatsu Photonics, Quantaaurus-Tau C11367). For phosphorescence lifetime measurements, a LED diode (340 nm, pulse width 1 ns, repetition rate 2 kHz) was used as the excitation light source. The analysis of the fluorescence and phosphorescence decay curves were carried out using the deconvolution method. Differential scanning calorimetry was performed on a METTLER TOLEDO DSC822e at heating and cooling rates of 10 K min⁻¹ under a nitrogen atmosphere. Powder X-ray diffraction measurements were performed on RIGAKU RINT-TTR III and carried out with Cu(K α) radiation from an X-ray tube with a 0.5 \times 10 mm² filament operated at 50 kV \times 300 mA (15 kW).

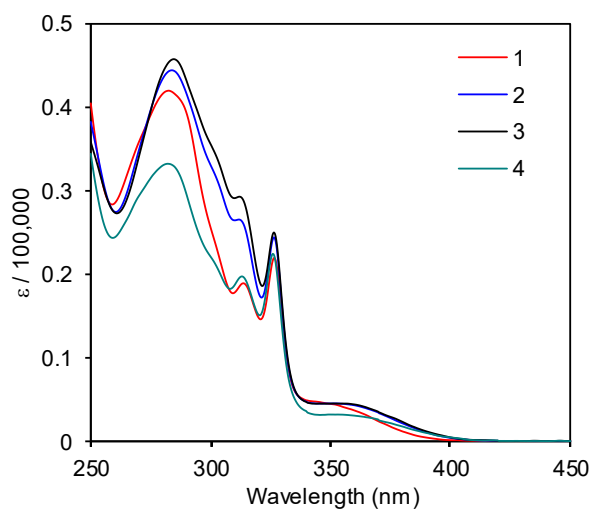


Fig S1 Absorption spectra of **1**, **2**, **3**, and **4** in DCM at 2.0×10^{-5} M.

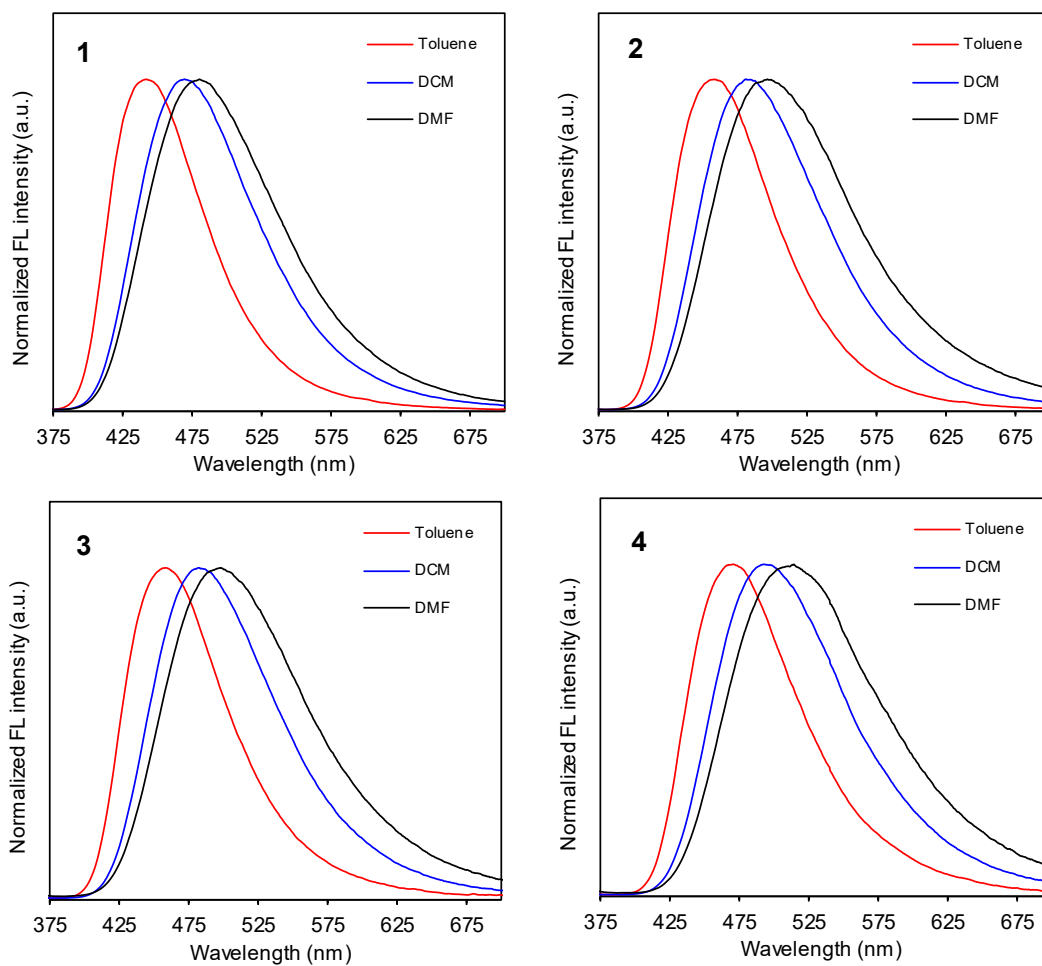


Fig S2 Fluorescence spectra (ex. 350 nm) of **1**, **2**, **3**, and **4** in toluene, DCM, and DMF at 2.0×10^{-6} M.

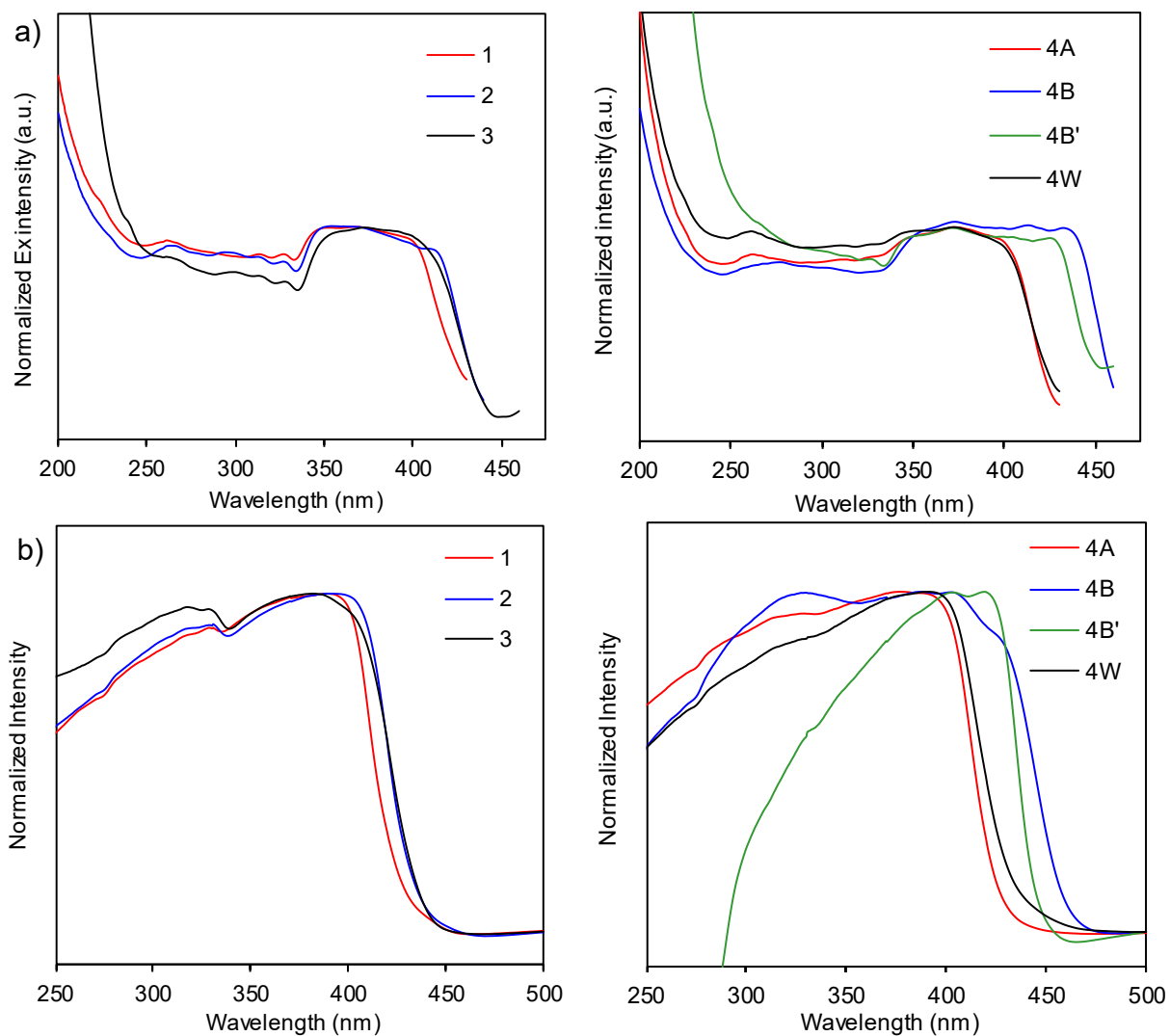


Fig S3 (a) Excitation spectra (monitored at emission maxima) and (b) diffuse reflection spectra of **1**, **2**, and **3** (left), and **4A**, **4B**, **4B'**, and **4W** (right) in crystal solid state.

Compared to **4A** and **4W**, the excitation band in **4B** was shifted bathochromically. This bathochromic shift coincided with that found in fluorescence spectra (Fig. 4a and 4b), indicating the **4B** molecule adopts a flat conformation to enhance the π -stacking interactions. Similar bathochromic shift was found also in diffuse reflection spectra.

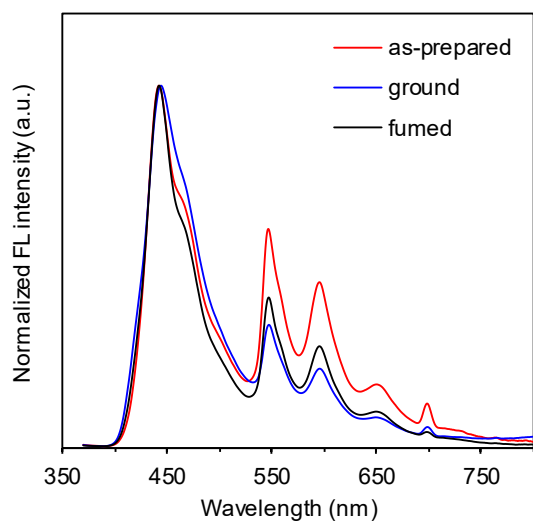


Fig. S4 Steady-state fluorescence spectra (ex. 350 nm) of **3** in the as-prepared, ground, and fumed solid state.

In **3** the spectra was not changed significantly by mechanical grinding and subsequent chloroform-vapor-fuming.

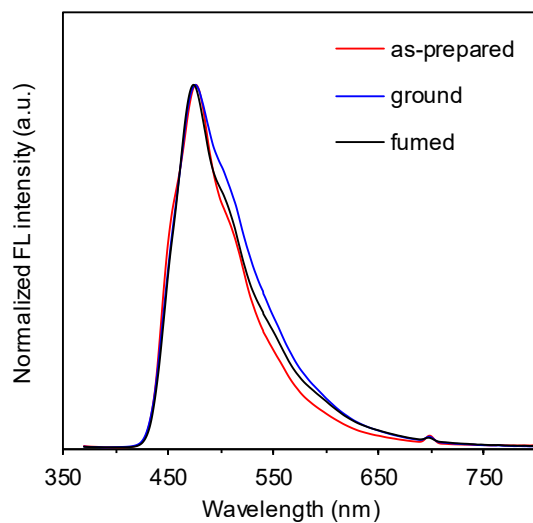


Fig. S5 Steady-state fluorescence spectra (ex. 350 nm) of **4B** in the as-prepared, ground, and fumed solid state.

In **4B**, the spectral shape was hardly changed by mechanical grinding and subsequent chloroform-vapor-fuming.

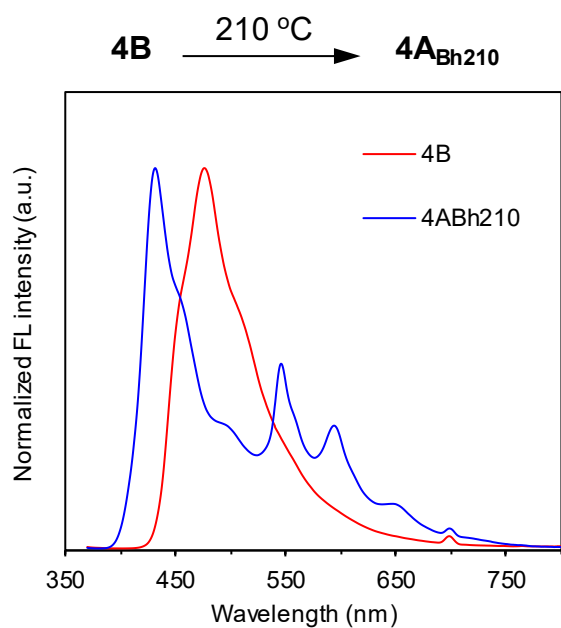


Fig. S6 Steady-state fluorescence spectral change in **4B** before and after heating at 210 °C.

A phase transition from **4B** to **4A_{Bh210}** was proceeded by heating at 210 °C (above melting point) and subsequent cooling to room temperature. For the compound number **4A_{Bh210}**, the capital plan character “**4A**” indicates the final crystal state (**4A**), and the subscript character “**Bh210**” indicates the starting crystal state (**4B**) and the stimulation conditions of heating at 210 °C (**h210**).

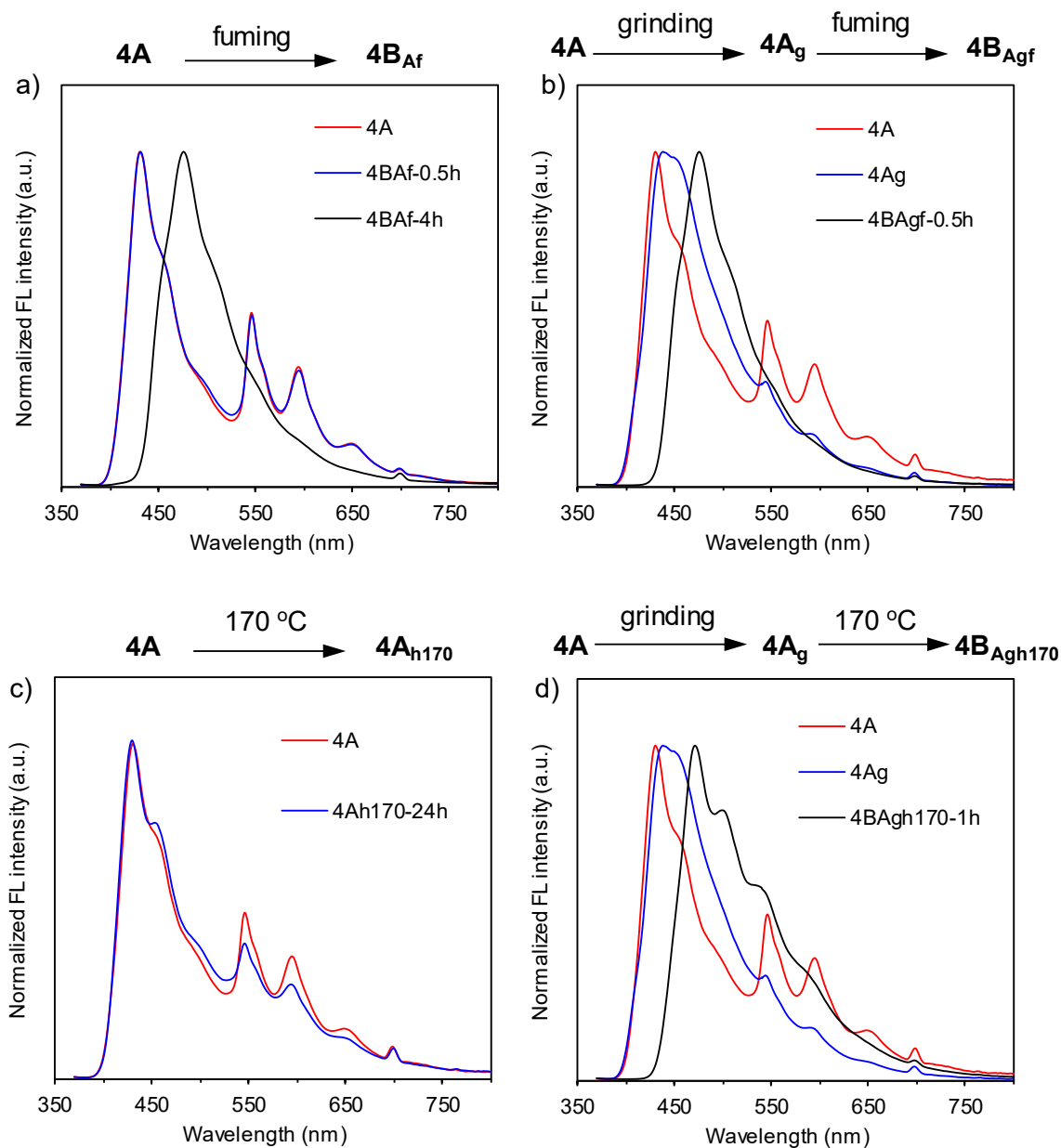


Fig. S7 Steady-state fluorescence spectral change in **4A** before and after external stimulus: (a) chloroform-vapor-fuming for 0.5 and 4 h, (b) mechanical grinding and subsequent chloroform-vapor-fuming for 0.5 h, (c) heating at 170 °C for 24 h, and (d) mechanical grinding and subsequent heating at 170 °C for 1 h.

For the compound numbers, the capital plan character indicates the final crystal state, and the subscript character indicates the starting crystal state and the stimulation conditions: e.g., for **4B_{Agh170}**, the capital plan character “**4B**” indicates the final crystal state (**4B**), and the subscript character “**Agh170**” indicates the starting crystal state (**4A**) and the stimulation conditions of grinding (**g**) and heating at 170 °C (**h170**).

A phase transition from **4A** to **4B** was proceeded by heating at 170 °C or vapor-fuming, which was accelerated by pretreatment of mechanical grinding. This change is governed thermodynamically.

In **4Ag**, the mechanical grinding treatment provided a broadened fluorescence band together with a shift to longer wavelength, which suggests a defect structure.

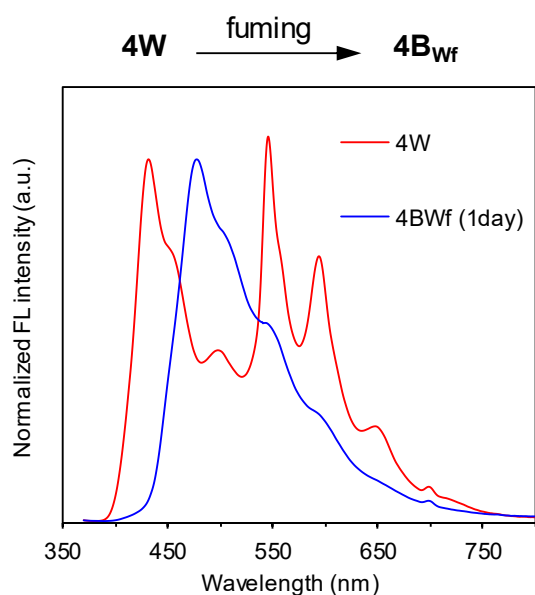


Fig. S8 Steady-state fluorescence spectral change in **4W** before and after chloroform-vapor-fuming.

A phase transition from **4W** to **4B_{wf}** was proceeded by vapor-fuming for 1 day. This phase transition rate was slower than that of change from **4A** to **4B** under the same vapor-fuming conditions (Fig. S7a).

For the compound number **4B_{wf}**, the capital plan character “**4B**” indicates the final crystal state (**4B**), and the subscript character “**w_f**” indicates the starting crystal state (**4W**) and the stimulation conditions of vapor-fuming (**f**).

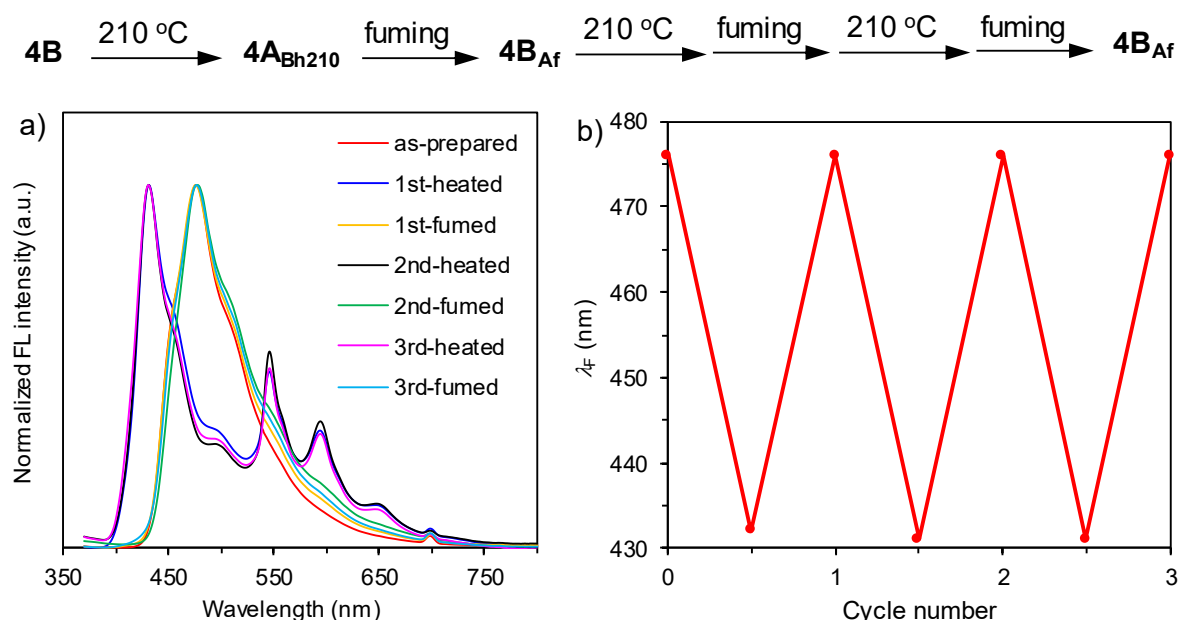


Fig. S9 (a) Fluorescence-phosphorescence switching between **4A** and **4B** by repeated heating (210 °C)–fuming (chloroform vapor) process starting from **4B**. The data in as-prepared (**4B**) and first-heated state (**4A_{Bh210}**) are same data in Fig. S6. (b) Plot of the fluorescence band by repeated heating–fuming process.

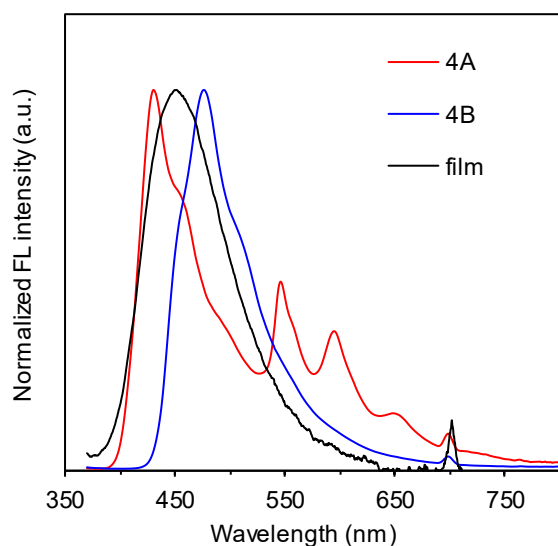


Fig. S10 Steady-state fluorescence (excited at 350 nm) of **4** in the crystal solid **A4** and **4B** state and in the PMMA film state (1 wt-%).

The phosphorescence could not be observed in the monomeric dispersed film state, indicating an importance of aggregation on the phosphorescence.

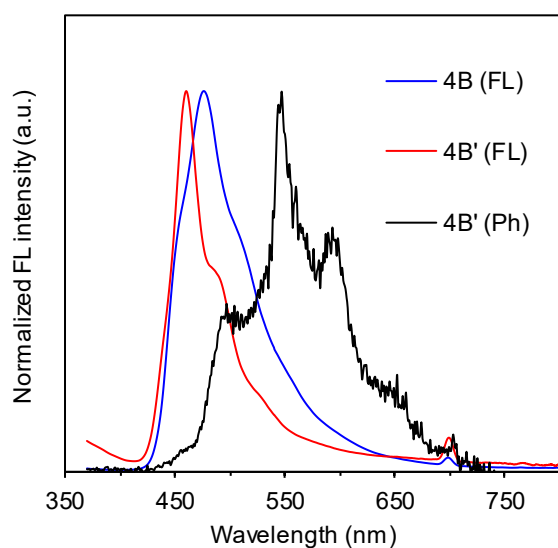


Fig. S11 Comparison of steady-state fluorescence spectra of **4B'** with **4B** together with phosphorescence spectrum of **4B'** in the crystal solid state (excited at 350 nm).

The **4B'** sample, which was obtained by recrystallization from boiling toluene as long and fine fibers, is phosphorescence-inactive as similar to **4B**, although the fluorescence band of **4B'** (460 nm) appeared at the shorter wavelength region compared to **4B** (476 nm). The difference would be ascribed to the slightly change of crystal packing structure arising from the inclusion of toluene molecules used as recrystallization solvent (Fig. 24 and the comment in the caption).

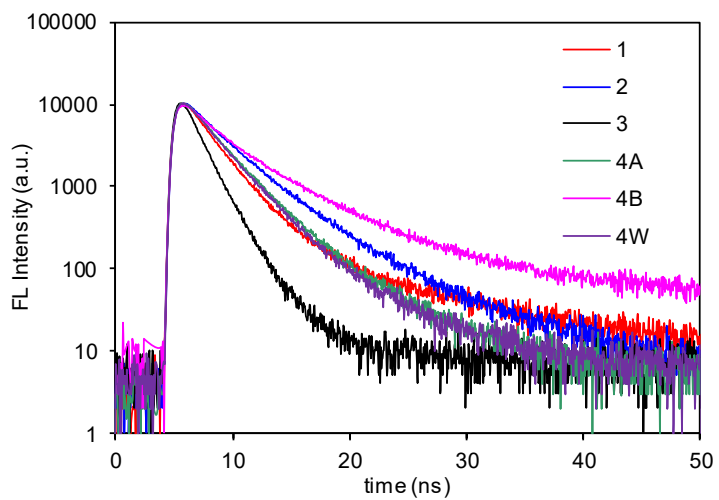


Fig. S12 Fluorescence decay curves of **1**, **2**, **3**, **4A**, **4B**, and **4W** (monitored at emission maxima) with excitation at 340 nm.

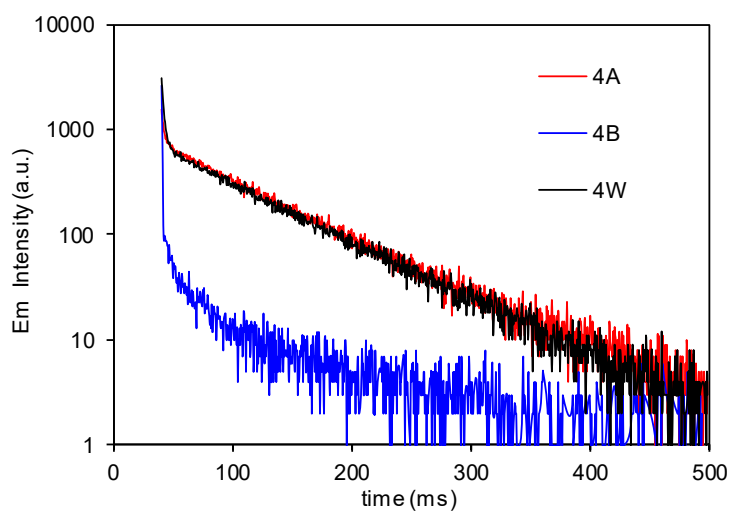
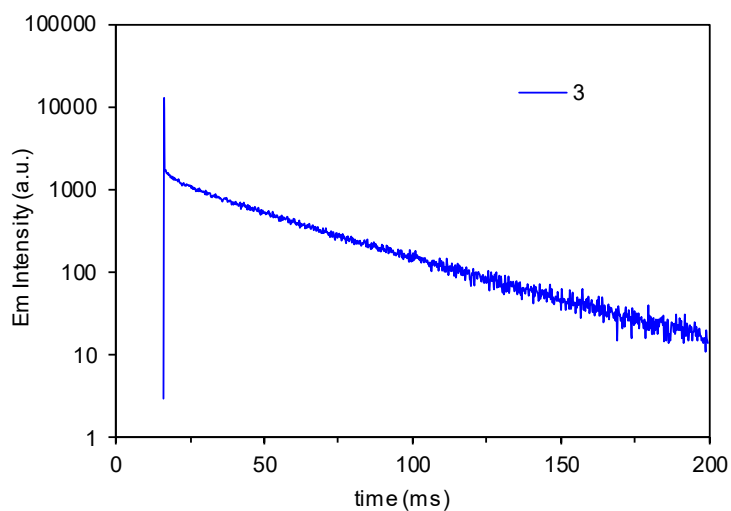


Fig. S13 Phosphorescence decay curves of **3**, **4A**, **4B**, and **4W** (monitored at 550 nm) with excitation at 340 nm.

Table S1 Spectral data of **1**, **2**, **3**, and **4** in solution state

Comp.	Solv.	λ_{abs} (nm)	ϵ	λ_{em} (nm)	Φ_{F}^a
1	Toluene	355 (sh)	3,644	442	0.028
		327	23,576		
		314	19,717		
		283	39,120		
	DCM	352 (sh)	4,387	470	0.044
		327	21,965		
		314	18,928		
		283	42,066		
	DMF	350 (sh)	4,817	480	0.042
		326	20,778		
		312	19,101		
		284	41,083		
2	Toluene	356 (sh)	3,328	458	0.039
		327	24,563		
		314	24,215		
		283	37,374		
	DCM	356 (sh)	4,472	482	0.048
		327	24,468		
		312	26,603		
		284	44,520		
	DMF	353 (sh)	4,474	496	0.053
		326	21,476		
		312	25,501		
		285	39,337		
3	Toluene	357 (sh)	5,210	458	0.009
		327	37,674		
		314	39,888		
		284	57,752		
	DCM	357 (sh)	4,484	483	0.013
		327	24,964		
		312	29,248		
		285	45,712		
	DMF	354	4,631	498	0.014
		326	21,738		
		313	27,203		
		286	39,145		
4	Toluene	365 (sh)	2,962	470	0.012
		327	28,208		
		314	23,096		
		283	35,586		
	DCM	357 (sh)	3,135	495	0.021
		326	22,417		
		313	19,715		
		282	33,206		
	DMF	358 (sh)	3,769	512	0.012
		326	22,085		
		313	21,641		
		284	34,816		

^a Determined relative to quinine sulfate (Φ_{F} 0.55, ex 350 nm) in 1 N sulfuric acid.

Table S2 Spectral data of **1**, **2**, **3**, and **4** in the crystal solid state

Comp.	Fluorescence			Phosphorescence		
	λ_F (nm)	Φ_F^a	τ_F (ns)	λ_P (nm)	Φ_P^a	τ_P (ms) ^b
1	428	0.065	7.3 (430) ^c	549, 598, 650 (sh)	-	193
2	441	0.090	4.3 (430) ^c	546, 592, 650 (sh)	-	77
3	442	0.030	1.6 (430) ^c	547, 595, 651	0.038	40
3^d	439	<i>e</i>	<i>e</i>	-	-	-
4A	431	0.051	3.4 (430) ^c 6.2 (455) ^c 8.4 (480) ^c	546, 595, 650	0.033	79
4A^d	451	<i>e</i>	<i>e</i>	-	-	-
4A_{h170}	430	0.037	-	546, 594, 649	0.020	-
4A_g	438	0.046	3.8 (430) ^c 5.3 (455) ^c 10.5 (480) ^c	546, 595, 650	0.019	54
4A_{Bh210}	432	0.046	<i>e</i>	546, 594, 649	0.041	<i>e</i>
4B	476	0.066	10.6 (475) ^c 8.7 (500) ^c 10.8 (540) ^c	554, 598, 658 (sh)	-	8
4B^e	460	0.040	<i>e</i>	547, 595, 650 (sh)	-	15
4B_{Af}	476	0.110	<i>e</i>	547, 596, 650 (sh)	-	-
4B_{Agf}	476	0.110	<i>e</i>	554, 604, 660 (sh)	-	-
4B_{Agh170}	471	0.060	10.0 (475) ^c 6.8 (500) ^c 11.4 (540) ^c	550, 597, 650 (sh)	-	-
4B_{wf}	478	0.108	<i>e</i>	547, 595, 650 (sh)	-	-
4W	432	0.036	3.1 (430) ^c	546, 595, 650	0.055	77
(4A_{h210})						

^a Absolute fluorescence and phosphorescence quantum yields determined by an integrating sphere system.

^b Monitored at 550 nm. ^c Value in the parenthesis is monitored wavelength. ^d 1 wt-% PMMA film. ^e Not measured.

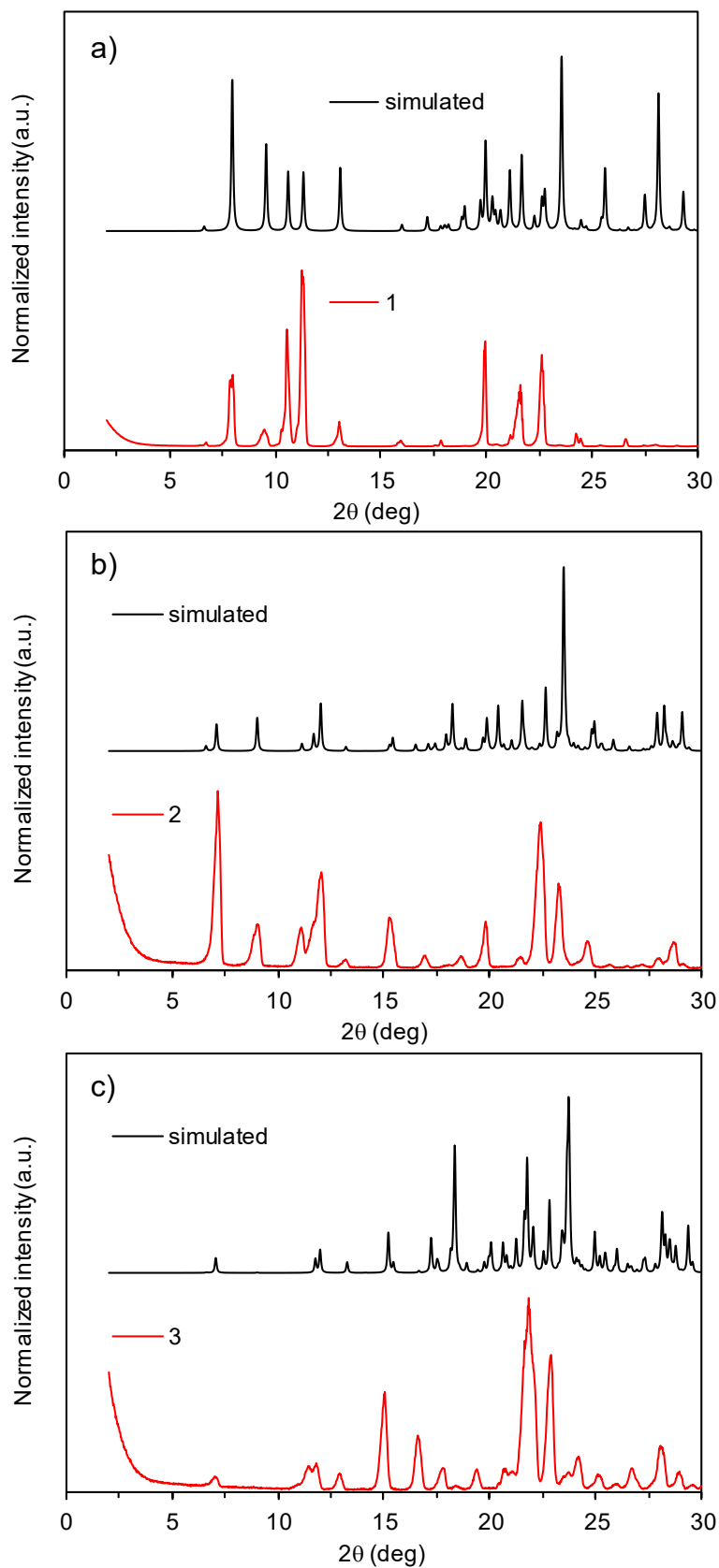


Fig. S14 Powder XRD patterns of (a) **1**, (b) **2**, and (c) **3** in the crystal solid state and the simulated powder patterns derived from a single crystal.

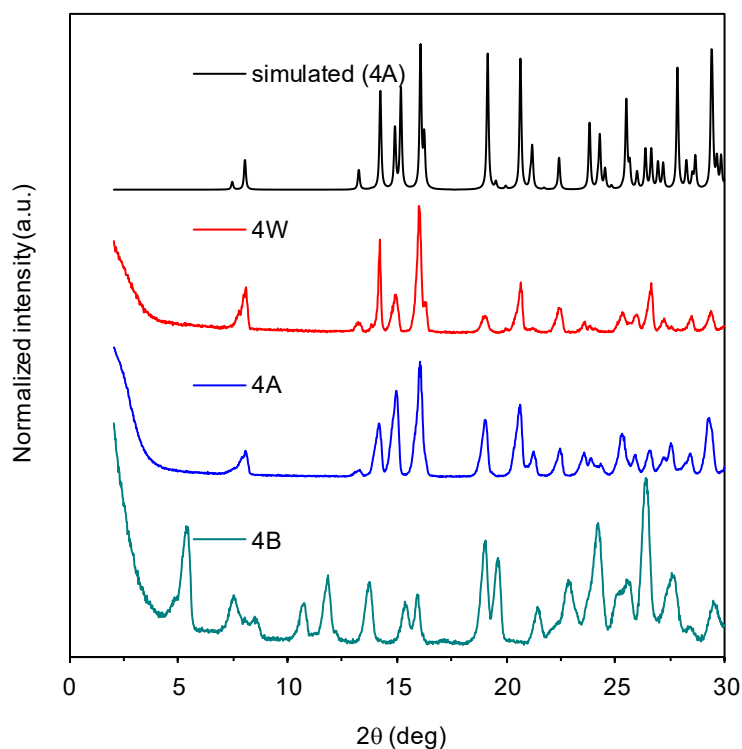


Fig. S15 Powder XRD patterns of **4A**, **4B**, and **4W**, and the simulated powder pattern derived from a single crystal of **4A**.

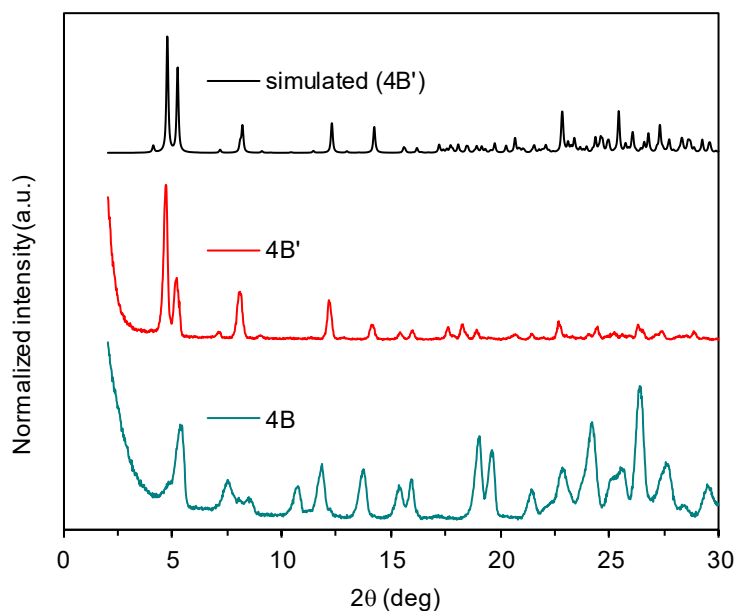


Fig. S16 Powder XRD patterns of **4B** and **4B'**, and the simulated powder pattern derived from a single crystal of **4B'**. The single crystal of **4B'** was obtained by recrystallization from boiling toluene.

The XRD pattern of **4B** is similar to that of **4B'**, which differs from **4A** (Fig. S15), indicating that **4B** has a similar crystal packing structure of **4B'** bearing one-dimensional parallel stacking mode (Fig. S24).

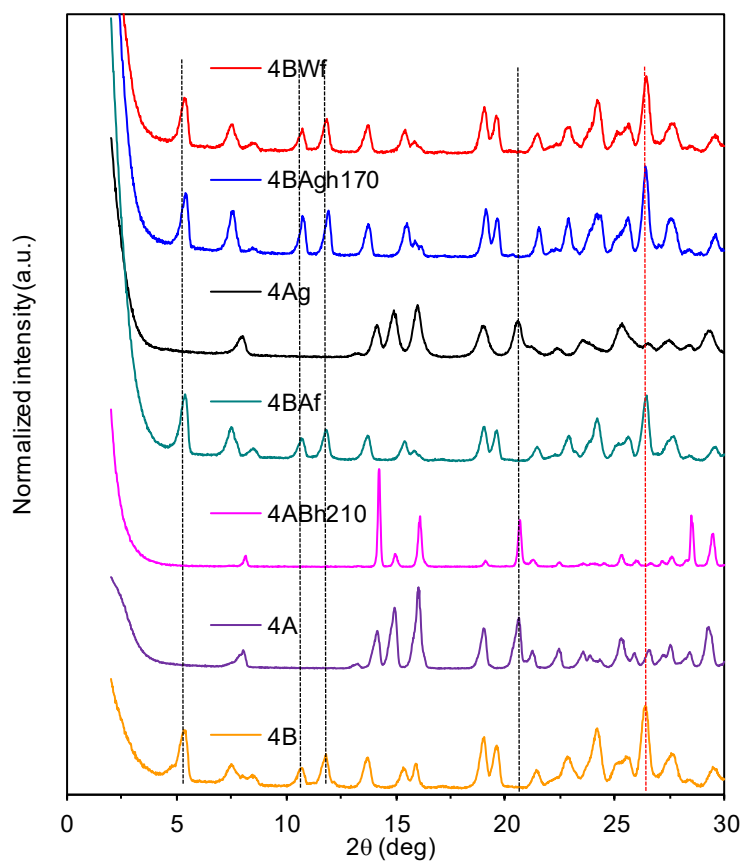


Fig. S17 Powder XRD patterns of **4A**, **4B**, **4A_{Bh210}**, **4A_f**, **4A_g**, **4A_{gh170}**, and **4B_{wf}**.

In **4A**, careful comparison of XRD traces of before and after (**4A_g**) mechanical grinding indicates a slight broadening of the reflections, which suggests a defect structure.

The **4B** samples (**4B**, **4A_f**, **4A_{gh170}**, and **4B_{wf}**) tend to indicate the enhanced reflection around 26.5 deg (ca. 3.35 Å), compared to the **4A** samples (indication by red dotted line). The reflection is attributed to the π -stacking interactions, which are found in single crystal structures of **1**, **2**, **3**, and **4A**. The finding suggests that the **4B** molecule adopts more flat conformation to enhance the π -stacking interactions compared to **4A**.

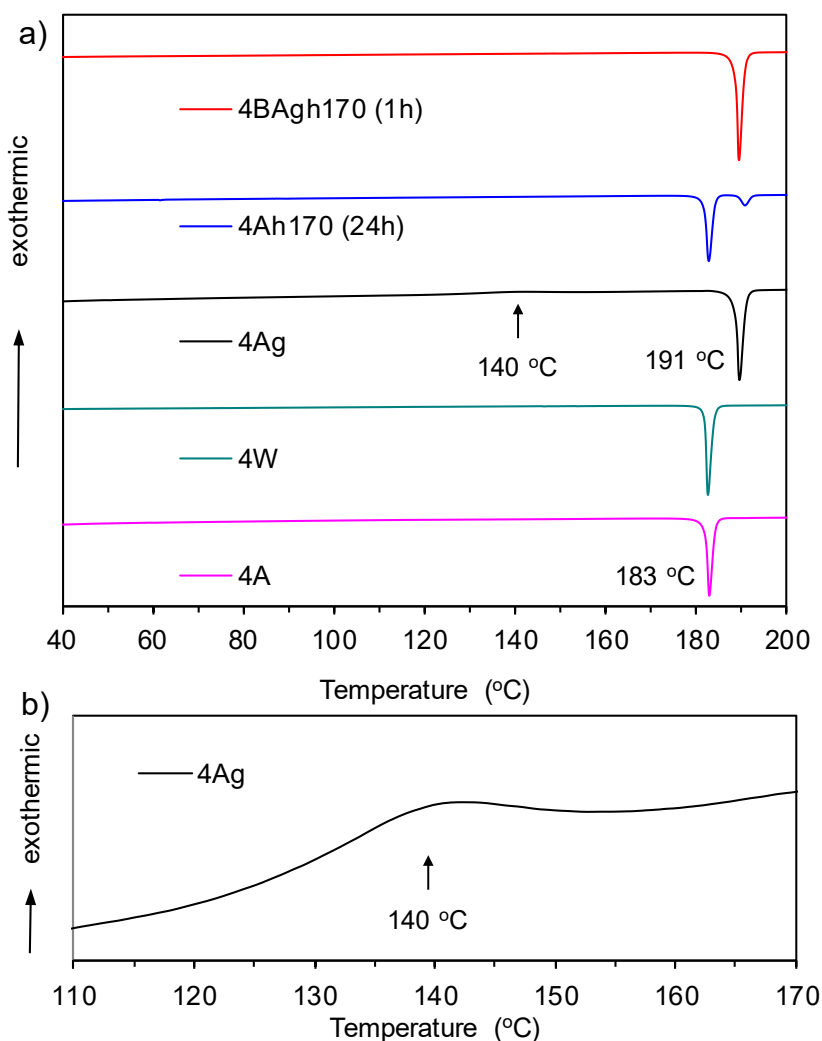


Fig. S18 (a) DSC curves of **4A** before and after external stimulus in the first heating step at rate of $10\text{ }^{\circ}\text{C min}^{-1}$: **4W** by heating at $210\text{ }^{\circ}\text{C}$, **4A_g** by grinding, **4A_{h170}** by heating at $170\text{ }^{\circ}\text{C}$ (24 h), and **4B_{Agh170}** by grinding and subsequent heating at $170\text{ }^{\circ}\text{C}$ (1 h). (b) The zooming of DSC curve of **4A_g**.

In **4A_g**, a phase transition temperature was observed at $140\text{ }^{\circ}\text{C}$, which was observable reliably and reproducibly. During this DSC measurement, **4A** was changed to **4B** above the transition temperature, as supported by an appearance of melting point at $190\text{ }^{\circ}\text{C}$.

The phase transition from **4A** to **4B** was proceeded very slightly by heating at $170\text{ }^{\circ}\text{C}$, which was accelerated by pre-treatment of mechanical grinding. This change is governed thermodynamically.

In **4A_{h170}**, the trace change from **4A** to **4B** was supported by this DSC trace, which showed the unchanged melting point ($183\text{ }^{\circ}\text{C}$) of **4A** along with a newly generated trace endothermic peak ($191\text{ }^{\circ}\text{C}$) corresponding to the melting point of **4B**.

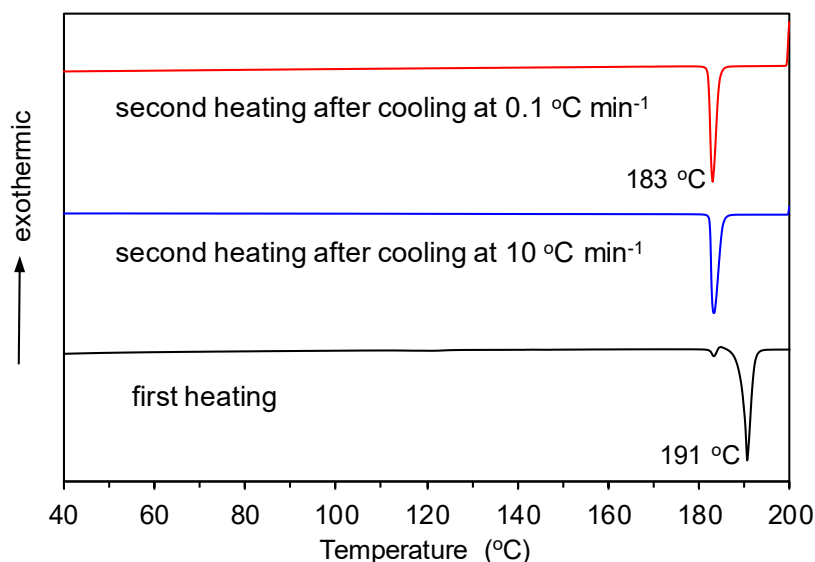


Fig. S19 DSC curves of **4B** in the first and second heating steps at heating rate of 10 °C min^{-1} . The second heating step was performed after cooling step at the different cooling rate of 0.1 and 10 °C min^{-1} .

In the first heating step, a weak endothermic peak at 183 °C was found in addition to the melting point (191 °C) of **4B**, indicating that **4B** contains a trace amounts of **4A**. In the second heating step, only the melting point (183 °C) of **4A** was observed even in the slow cooling rate of 0.1 °C min^{-1} . These results indicate that the transition from **4B** and **4A** is induced by heating (above melting point) and the subsequent cooling.

Table S3 Thermal analysis data obtained from DSC traces

comp.	T_m (°C)	ΔH (kJ mol ⁻¹)	comp.	T_m (°C)	ΔH (kJ mol ⁻¹)
1	218	-36.7	4W	183	-29.9
2	293	-38.2	4A_g	140 ^b	6.65
				191 ^b	-38.2
3	300	-41.6	4B_{Agf}	191	-40.0
4A	183	-28.5	4A_{h170}	183	-25.7
				191 ^c	-4.85
4B	183 ^a	-1.9	4B_{Agh170}	191	-40.2
	191	-37.8			

^a This weak endothermic peak is based on the contamination of trace amounts of **4A**.

^b This DSC trace indicated an exothermic peak at 140 °C and a melting point at 191 °C corresponding to **4B** but not to **4A**, indicating a phase transition from **4A** to **4B** at 140 °C during this DSC heating step

^c This newly generated weak endothermic peak is based on the slight phase transition (from **4A** to **4B**) by heating at 170 °C .

Single crystal X-ray diffraction analysis

The single crystals for the X-ray diffraction analysis were obtained by the slow diffusion of hexane into the dichloromethane solution in **1** (colorless prisms), by heating (70 °C) of DMF solution and subsequent cooling to room temperature in **2** (colorless needles) and **3** (colorless needles), by the slow diffusion of hexane into the 1,1,2,2-tetrachloroethane solution in **4A** (colorless prisms), and by heating (110 °C) of toluene solution and subsequent cooling to room temperature in **4B'** (pale yellow long and fine needles).

All measurements were made on a Rigaku Saturn 724 or HyPix-6000 HE diffractometer using graphite monochromated Mo-K α radiation. Using Olex2¹, the structure was solved with the ShelXT² structure solution program using Intrinsic Phasing and refined with the ShelXL² refinement package using Least Squares minimization. The non-hydrogen atoms were refined anisotropically. Hydrogen atoms were refined using the riding model. Simulated powder patterns were generated with Mercury 3.8 from the structures determined by single crystal diffraction analyses.³

1 O. V. Dolomanov, L. J. Bourhis, R. J. Gildea, J. A. K. Howard and H. Puschmann, OLEX2: A complete structure solution, refinement and analysis program. *J. Appl. Cryst.*, 2009, **42**, 339–341.

2 G. M. Sheldrick, *Acta Cryst.*, 2015, **C71**, 3–8.

3 http://www.ccdc.cam.ac.uk/free_services/mercury/downloads/Mercury_3.8/.

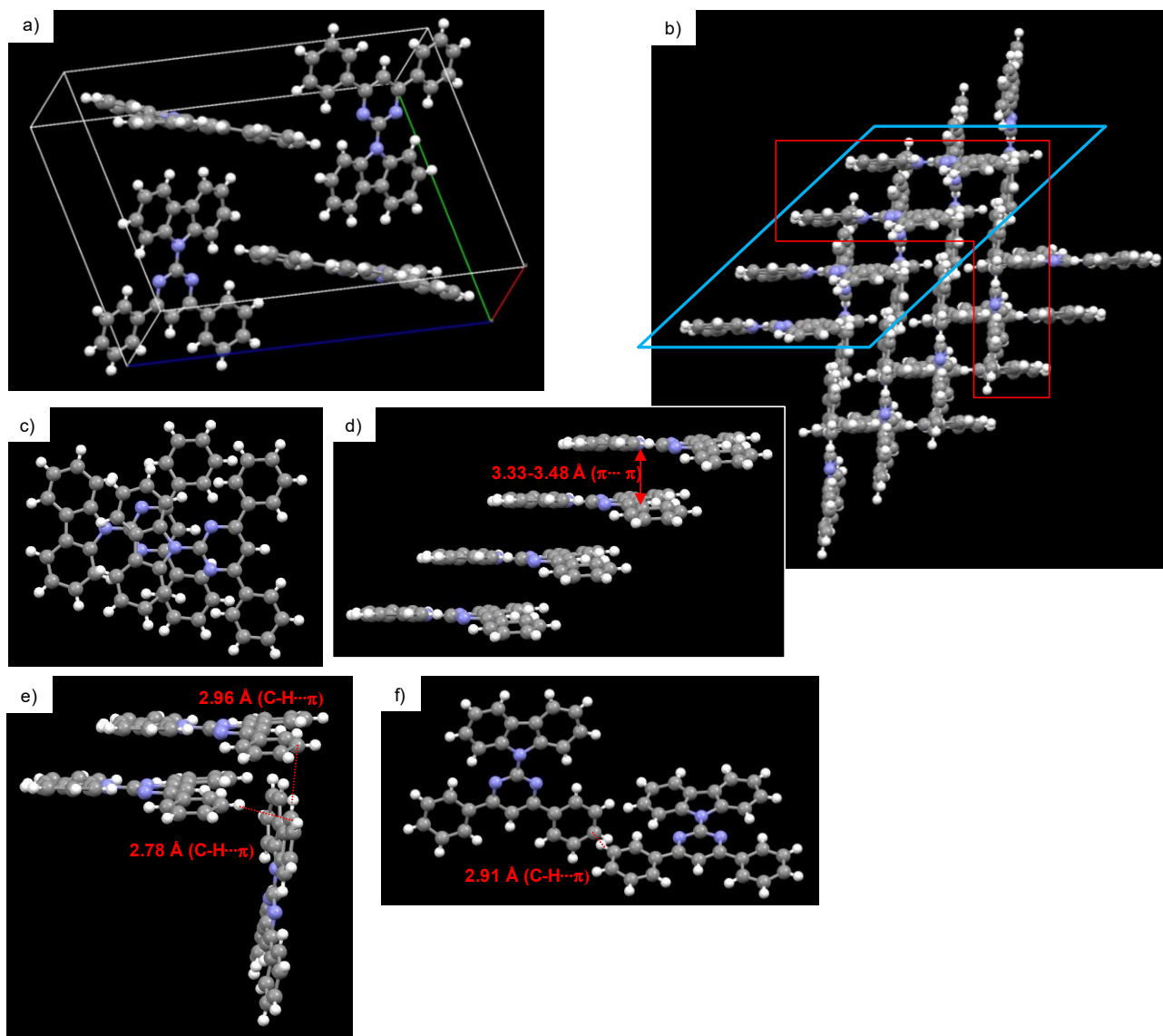


Fig. S20 Crystal structure of **1**: (a) unit cell packing, (b) three-dimensional packing, which is constructed by intertwining the one-dimensional stacking structures of the four molecules in the unit cell, (c) aggregate structure with parallel stacked arrangement, (d) one-dimensional stacking structure, which is a part of the three-dimensional packing shown in Fig S17b (indicated by blue region), (e) perpendicularly arranged L-shape structure, which is a part of the three-dimensional packing shown in Fig S17b (indicated by red region), and (f) two-dimensionally arranged packing structure created within the three-dimensional packing of Fig. S17b.

The crystal packing is constructed by π -stacking interactions in one-dimensional direction, by C-H \cdots π interactions in two-dimensional direction, and by intertwining the one-dimensional stacking structures through C-H \cdots π interactions in three-dimensional direction.

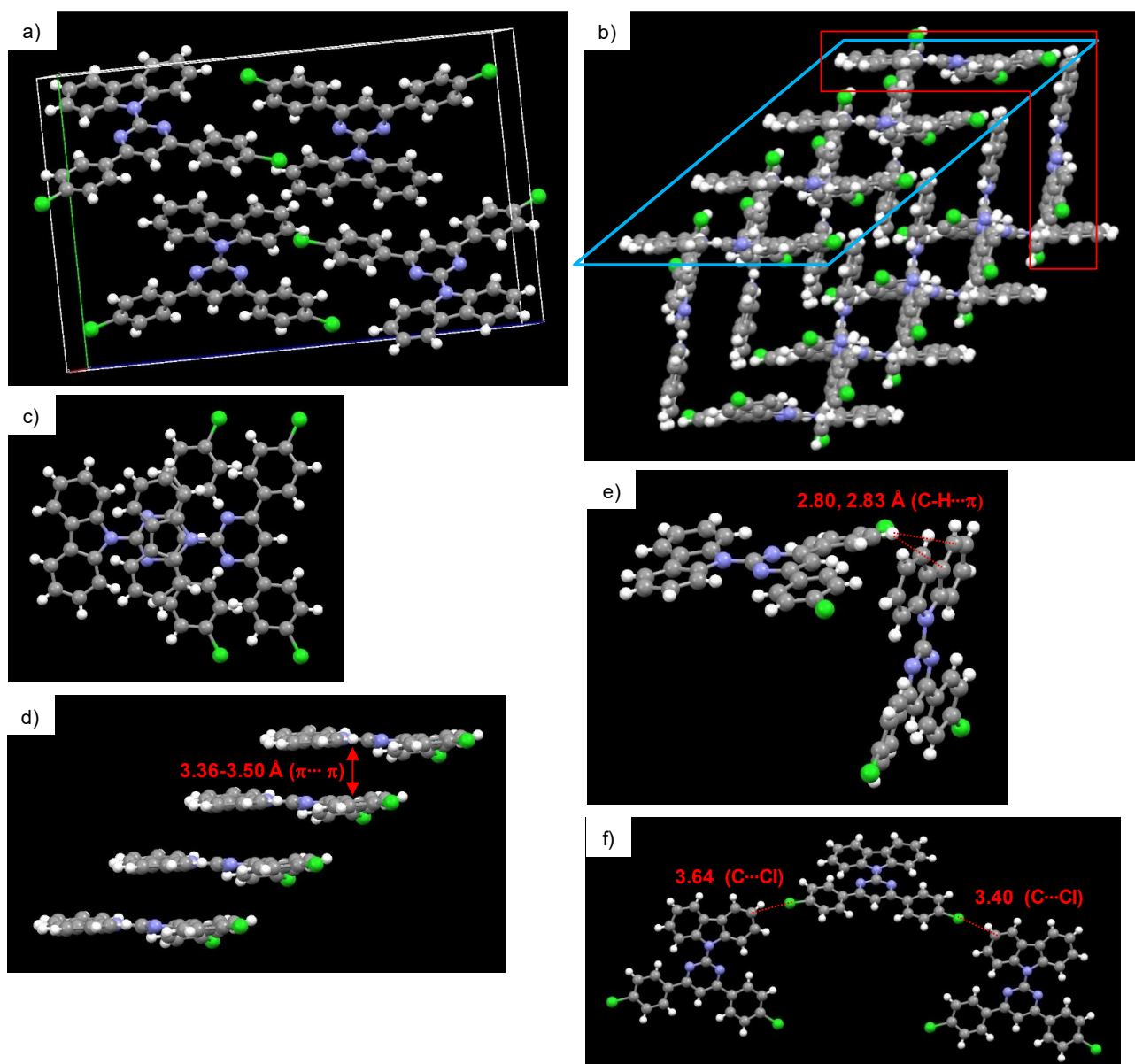


Fig. S21 Crystal structure of **2**: (a) unit cell packing, (b) three-dimensional packing, which is constructed by intertwining the one-dimensional stacking structures of the four molecules in the unit cell, (c) aggregate structure with parallel stacked arrangement, (d) one-dimensional stacking structure, which is a part of the three-dimensional packing shown in Fig S18b (indicated by blue region), (e) perpendicularly arranged L-shape structure, which is a part of the three-dimensional packing shown in Fig S18b (indicated by red region), and (f) two-dimensionally arranged packing structure created within the three-dimensional packing of Fig. S18b.

The crystal packing is constructed by π -stacking interactions in one-dimensional direction, by halogen interactions in two-dimensional direction, and by intertwining the one-dimensional stacking structures through C-H $\cdots\pi$ interactions in three-dimensional direction.

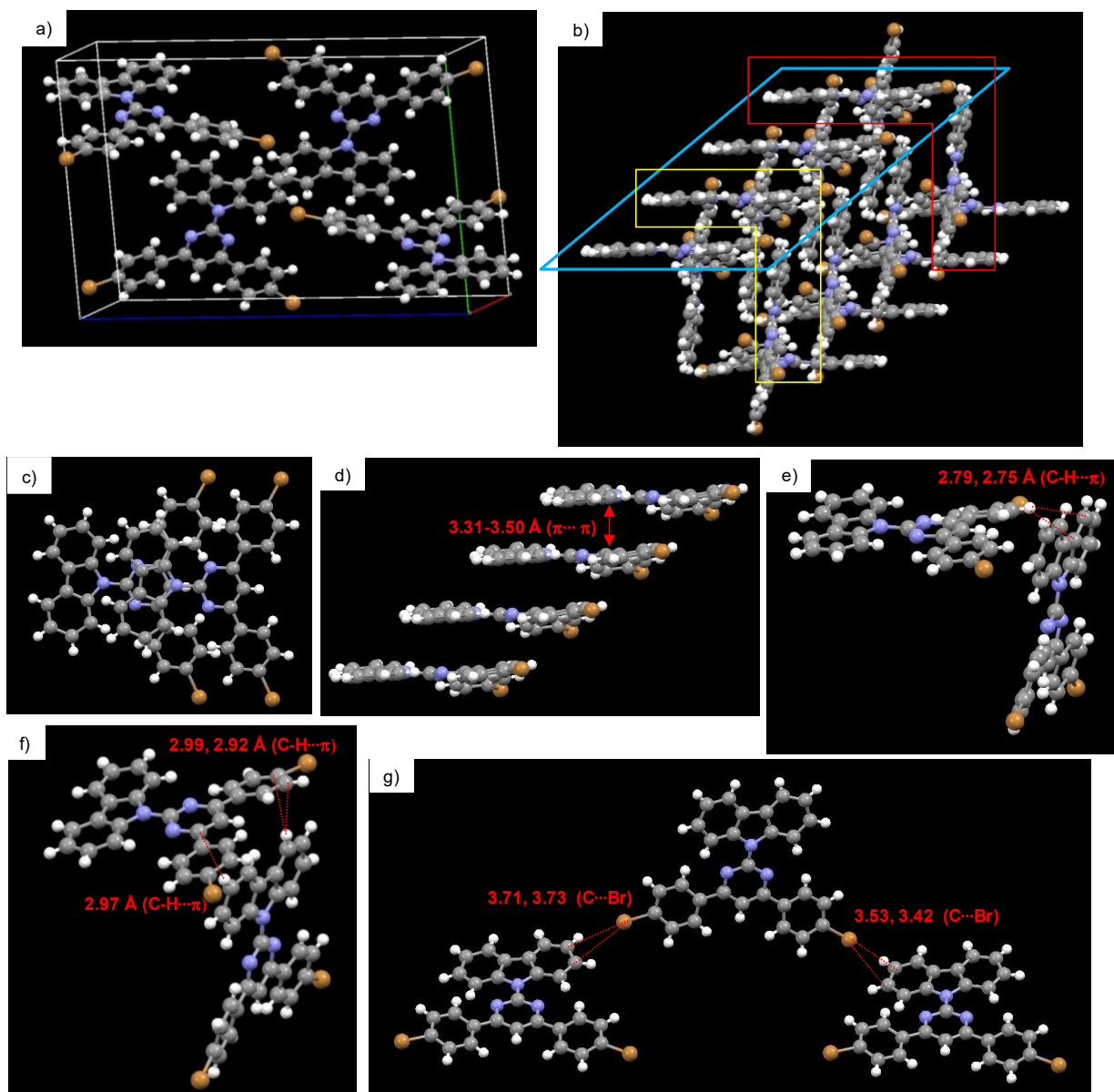


Fig. S22 Crystal structure of **3**: (a) unit cell packing, (b) three-dimensional packing, which is constructed by intertwining the one-dimensional stacking structures of the four molecules in the unit cell, (c) aggregate structure with parallel stacked arrangement (top view for Fig. 3a), (d) one-dimensional stacking structure, which is a part of the three-dimensional packing shown in Fig S19b (indicated by blue region) (the dimeric structure shown in Fig. 3a is a part of this one-dimensional stacking), (e) perpendicularly arranged L-shape structure as shown in Fig. 3b, which is a part of the three-dimensional packing shown in Fig S19b (indicated by red region), (f) another perpendicularly arranged L-shape structure, which is a part of the three-dimensional packing shown in Fig S19b (indicated by yellow region), and (g) two-dimensionally arranged packing structure created within the three-dimensional packing of Fig. S19b.

The crystal packing is constructed by π -stacking interactions in one-dimensional direction, by halogen interactions in two-dimensional direction, and by intertwining the one-dimensional stacking structures through C-H \cdots π interactions in three-dimensional direction.

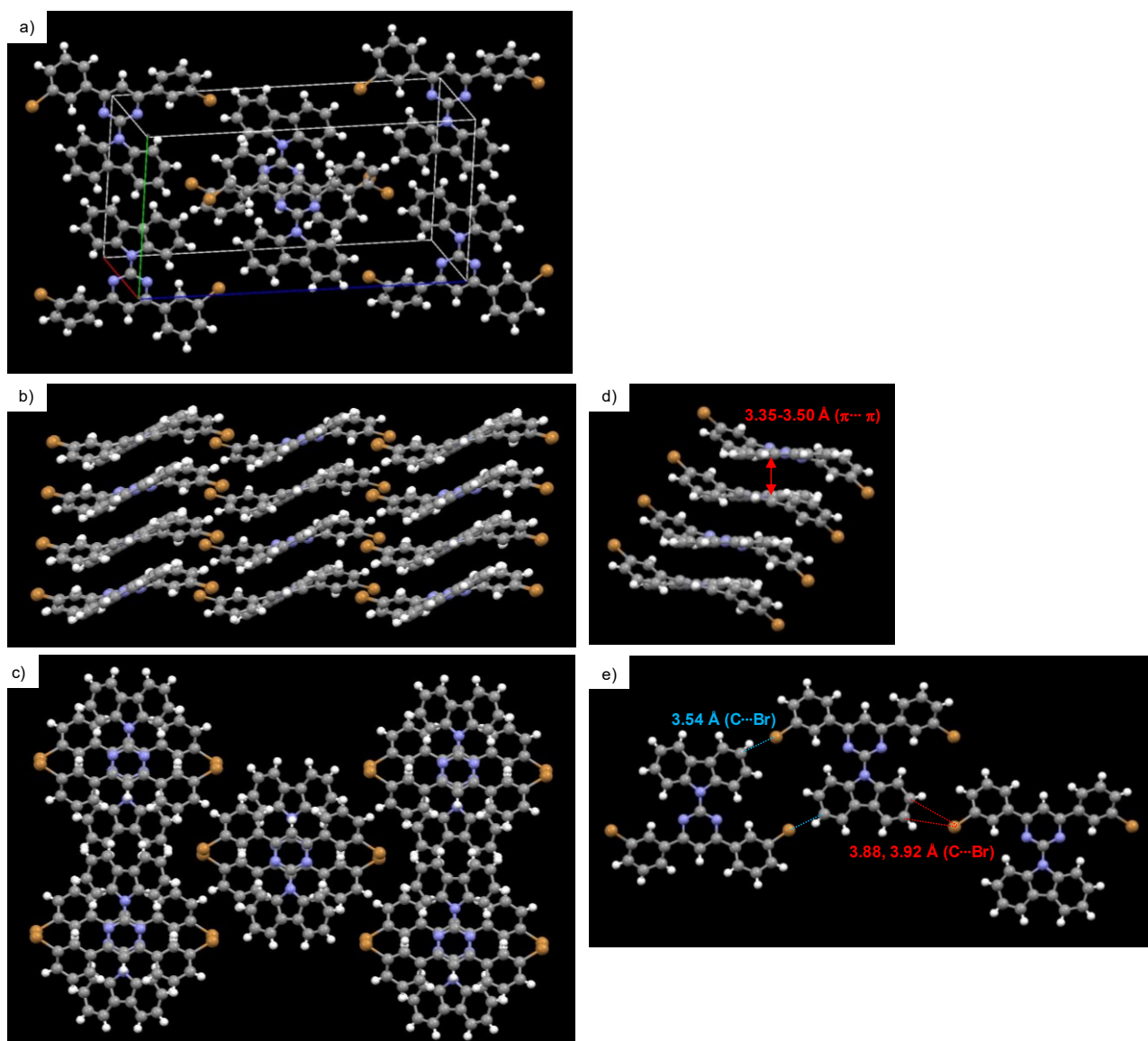


Fig. S23 Crystal structure of 4A: (a) unit cell packing, (b) side and (c) top views of three-dimensional packing, which is constructed by one-dimensional stacking structures of the six molecules in the unit cell, (d) one-dimensional stacking structure (the dimeric structure shown in Fig. 3c is a part of this one-dimensional stacking), (e) two-dimensionally arranged packing structure, which is a part of Fig. S20c.

The crystal packing is constructed by π -stacking interactions in one-dimensional direction and by halogen interactions in two-dimensional direction.

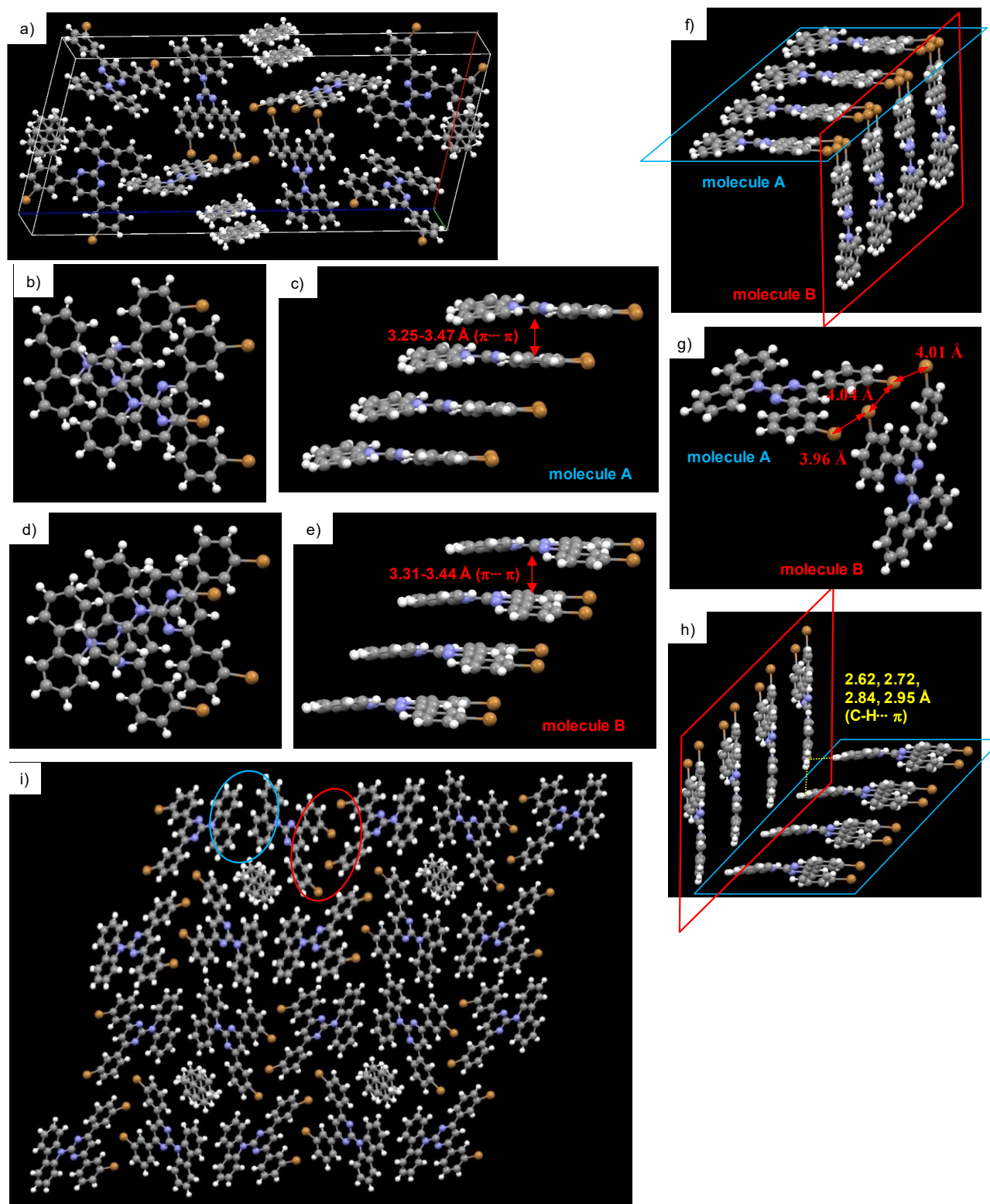


Fig. S24 Crystal structure of **4B'**, which is composed of two independent dye molecules A and B and of included solvent toluene molecules: (a) unit cell packing, (b) dimeric structure of molecule A with parallel stacked arrangement, (c) one-dimensional stacking structure of molecule A (the dimeric structure shown in Fig. S24b is a part of this one-dimensional stacking), (d) dimeric structure of molecule B with parallel stacked arrangement, (e) one-dimensional stacking structure of molecule B (the dimeric structure shown in Fig. S24d

is a part of this one-dimensional stacking), (f) (g) perpendicularly arranged L-shaped structure between bromine-substituted benzene moieties, which is constructed by intertwining of one-dimensional stacking structures shown in Fig S24c (indicated by blue region) and Fig. S24e (indicated by red region), (h) another perpendicularly arranged L-shaped structure between carbazole moieties, which is constructed by intertwining of the one-dimensional stacking structures shown in Fig S24c (indicated by blue region) and Fig. S24e (indicated by red region), and (i) two-dimensional view of crystal structure including toluene solvent molecules to indicate the L-shaped structures between bromine-substituted benzene moieties shown in Fig. S24f (indicated by red region) and between carbazole moieties shown in Fig. S24h (indicated by blue region).

In this crystal structure, toluene solvent molecules are included to show 4:1 stoichiometry of dye/toluene. In contrast to this solvent inclusion, **4B** did not have any solvent molecules used in recrystallization (chloroform and hexane), as checked by elemental analysis and ^1H NMR data as well as the finding that **4B** can be obtained from **4A** by external stimulation without solvent-vapor fuming. Probably, these results with and without solvent molecules is reflected in the slightly difference in photophysical and morphological properties between **4B** and **4B'** (Figs. S11 and S16).

Both molecules A and B has a flat conformation, which is attributed to the out-out conformation (Fig. S25a). The bathochromic shift in the fluorescence band of **4B'** relative to **4A** can be explained by this flat conformation. Also, this bathochromic shift can be supported by the slipped tacking mode found in the dimeric structures (Fig. 24b and 24d), in which the carbazole-pyrimidine connected moiety in one molecule is overlapped with the pyrimidine-benzene connected moiety in the other molecule.

In the L-shaped structure (Fig. 24f and 24g), the four bromine atoms are oriented alternatively to minimally reduce the steric repulsion. The distance between bromine atoms ($>3.96 \text{ \AA}$) is longer than the sum of van der Waals radius of bromine atom (3.70 \AA). Thus, this crystal packing structure rules out the opportunity for intermolecular halogen interactions, leading to the observed inactivity in phosphorescence.

Table S4 Selected data for the single crystals of **1**, **2**, **3**, **4A**, and **4B'**

data		1	2	3	4A	4B'
Monomer:						
molecular symmetry		asymmetry	asymmetry	asymmetry	symmetry	asymmetry (two independent molecules A and B)
bond length (Å)	pyrimidine-carbazole	1.407	1.420	1.408	1.392	A: 1.400, B: 1.396
	pyrimidine-benzene	1.487, 1.492	1.495, 1.505	1.477, 1.492	1.484	A: 1.491, 1.494, B: 1.490, 1.494
dihedral angle (°) ^a	pyrimidine-carbazole	3.47	5.23	6.26	15.86	8.61 (A: 9.06, B: 8.16)
	pyrimidine-benzene	7.05	10.25	11.27	26.40	2.49 (A: 2.65, B: 2.34)
density (g cm ⁻³)		1.374	1.442	1.741	1.661	1.691
Stacked dimer:						
arrangement		parallel	parallel	parallel	anti-parallel	parallel
intermolecular interactions (Å) ^a	pyrimidine-carbazole (π⋯π)	3.313, 3.470, 3.488, 3.496	3.361, 3.443, 3.484, 3.488, 3.500, 3.500	3.333, 3.369, 3.394, 3.402, 3.419, 3.477, 3.483	3.500, 3.500	A: 3.360, 3.403, B: 3.392
	pyrimidine-benzene (π⋯π)					A: 3.350, 3.421, 3.427, 3.464, B: 3.361, 3.368, 3.395, 3.413, 3.435
	carbazole-benzene (π⋯π)				3.352, 3.352, 3.375, 3.375	A: 3.254, 3.350, 3.364, 3.467
	carbazole-carbazole (π⋯π)					A: 3.339, 3.358, 3.405, B: 3.311, 3.355, 3.358
	benzene-benzene (π⋯π)		3.399, 3.423	3.348, 3.369		

Packing:						
intermolecular interactions (Å)	intertwining	2.783, 2.960	2.803, 2.825	2.748, 2.793,	3.470 ($\pi\cdots\pi$)	2.619, 2.724,
	one-dimensional stacking	(C-H $\cdots\pi$)	(C-H \cdots Cl)	2.919, 2.968,		2.838, 2.949 (C-H $\cdots\pi$)
				2.986		
				(C-H \cdots Br)		
	two-dimensional packing	2.914 (C-H $\cdots\pi$)	3.397, 3.640 (C \cdots Cl)	3.415, 3.528	3.535, 3.535,	
				3.707 3.727	3.880, 3.921	
				(C \cdots Br)	(C \cdots Br)	

^a Compared to the **2** molecule, the **3** molecule has slightly bent structure, nevertheless these two molecules have comparable π -stacking contacts in the stacked dimer structure. The bent structure is likely to reduce the π -stacking interactions, leading to the shorter phosphorescence lifetime (40 ms in **3**, and 77 ms in **2**), according to MUSIC concept: strong π -stacking interactions tend to stabilize triplet state, leading to a persistent phosphorescence (J. Yang, X. Zhen, B. Wang, X. Gao, Z. Ren, J. Wang, Y. Xie, J. Li, Q. Peng, K. Pu and Z. Li, *Nat. Commun.*, 2018, **9**, 840).

Table S5. Crystallographic data for **1**, **2**, **3**, and **4A**

	1	2	3	4A	4B'
CCDC number	1975638	1975640	1975643	1975644	1987804
diffractometer	Saturn 724	Saturn 724	HyPix-6000HF	HyPix-6000HF	HyPix-6000HF
formula	C ₂₈ H ₁₉ N ₃	C ₂₈ H ₁₇ Cl ₂ N ₃	C ₂₈ H ₁₇ Br ₂ N ₃	C ₂₈ H ₁₇ Br ₂ N ₃	C ₂₈ H ₁₇ Br ₂ N ₃ 0.25(C ₇ H ₈)
M	397.48	466.37	555.27	555.27	578.30
<i>T</i> [K]	123	123	123	123	100
crystal system	monoclinic	monoclinic	monoclinic	monoclinic	monoclinic
space group	<i>P</i> 2 ₁ / <i>n</i> (no. 14)	<i>P</i> 2 ₁ / <i>n</i> (no. 14)	<i>P</i> 2 ₁ / <i>n</i> (no. 14)	<i>I</i> 2/ <i>a</i> (no. 15)	<i>P</i> 2 ₁ / <i>n</i> (no. 14)
<i>a</i> [Å]	5.182 (2)	5.421 (3)	5.3634 (3)	7.5013 (4)	19.6547 (6)
<i>b</i> [Å]	16.682 (7)	15.895 (10)	15.7657 (7)	12.4477 (7)	5.3445 (3)
<i>c</i> [Å]	22.341 (10)	24.997 (16)	25.1499 (11)	23.8886 (11)	43.593 (2)
α [°]	90	90	90	90	90
β [°]	95.945 (11)	94.464 (14)	94.964 (4)	95.423 (4)	97.224 (4)
γ [°]	90	90	90	90	90
<i>V</i> [Å ³]	1920.8 (14)	2147 (2)	2118.64 (18)	2220.6 (2)	4542.8 (4)
<i>Z</i>	4	4	4	4	8
ρ_{calcd} [g cm ⁻³]	1.374	1.442	1.741	1.661	1.691
μ [mm ⁻¹]	0.817 (MoK α)	3.251 (MoK α)	3.850 (MoK α)	3.673(MoK α)	3.595
<i>F</i> (000)	832	960	1104	1104	2308
crystal size [mm ³]	0.20×0.12×0.06	0.15×0.02×0.01	0.30×0.03×0.02	0.18×0.06×0.04	0.3×0.01×0.01
reflections collected	19114	19431	17268	11179	38599
reflections unique	4311	4808	4838	2550	10375
<i>R</i> _{int}	0.0805	0.1057	0.0910	0.0375	0.0460
data [<i>F</i> ² > 2 σ (<i>F</i> ²)]	3661	3232	3587	2230	8653
parameters	280	298	298	151	659
goodness-of-fit	1.190	1.134	1.042	1.049	1.057
<i>R</i> 1/ <i>wR</i> ² [<i>F</i> ² > 2 σ (<i>F</i> ²)]	0.0988/0.214	0.1047/0.2499	0.0750/0.1928	0.0372/0.0819	0.0474/0.0838
<i>R</i> 1/ <i>wR</i> ² (all data)	0.1143/0.2269	0.1521/0.2921	0.0971/0.2062	0.0448/0.0848	0.0638/0.0885
Max Shift/error in final cycle	0.000	0.000	0.001	0.001	0.002

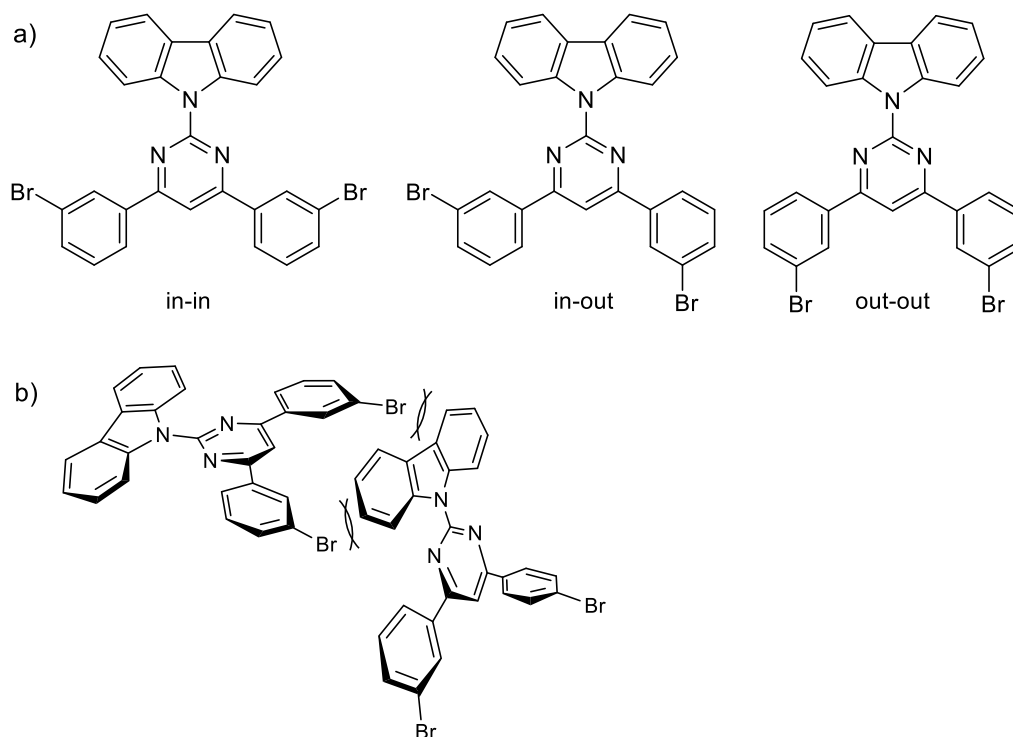


Fig. S25 (a) Three possible conformations (in-in, in-out, and out-out) for **4A** (in-in) and **4B** (out-out), and (b) a plausible L-shaped contact of out-out conformers with steric repulsion.

The out-out conformation in **4B** is not suitable for intertwining between the one-dimensional aggregate packing structures, because the bromine atoms in the meta-position sterically disturb the L-shaped contact with carbazole moiety found in dye **3** (Figs. 3b and S22e,f). This impossibility of intertwining rules out the opportunity for intermolecular halogen interactions, leading to the observed inactivity in phosphorescence.

Computer simulation analysis.

Theoretical calculations were performed using the Gaussian 09 program package.¹ Molecular properties in the electronic ground state were computed using the hybrid M06-2X DFT method. Geometry optimization was performed at the 6-31G(d) basis set. Frequency calculations on these optimized geometries revealed no imaginary frequencies.

1 M. J. Frisch, G. W. Trucks, H. B. Schlegel, G. E. Scuseria, M. A. Robb, J. R. Cheeseman, G. Scalmani, V. Barone, B. Mennucci, G. A. Petersson, H. Nakatsuji, M. Caricato, X. Li, H. P. Hratchian, A. F. Izmaylov, J. Bloino, G. Zheng, J. L. Sonnenberg, M. Hada, M. Ehara, K. Toyota, R. Fukuda, J. Hasegawa, M. Ishida, T. Nakajima, Y. Honda, O. Kitao, H. Nakai, T. Vreven, J. A. Montgomery, Jr., J. E. Peralta, F. Ogliaro, M. Bearpark, J. J. Heyd, E. Brothers, K. N. Kudin, V. N. Staroverov, R. Kobayashi, J. Normand, K. Raghavachari, A. Rendell, J. C. Burant, S. S. Iyengar, J. Tomasi, M. Cossi, N. Rega, J. M. Millam, M. Klene, J. E. Knox, J.

B. Cross, V. Bakken, C. Adamo, J. Jaramillo, R. Gomperts, R. E. Stratmann, O. Yazyev, A. J. Austin, R. Cammi, C. Pomelli, J. W. Ochterski, R. L. Martin, K. Morokuma, V. G. Zakrzewski, G. A. Voth, P. Salvador, J. J. Dannenberg, S. Dapprich, A. D. Daniels, Ö. Farkas, J. B. Foresman, J. V. Ortiz, J. Cioslowski and D. J. Fox, *Gaussian 09*, Revision D.01; Gaussian Inc.: Wallingford CT, 2009.

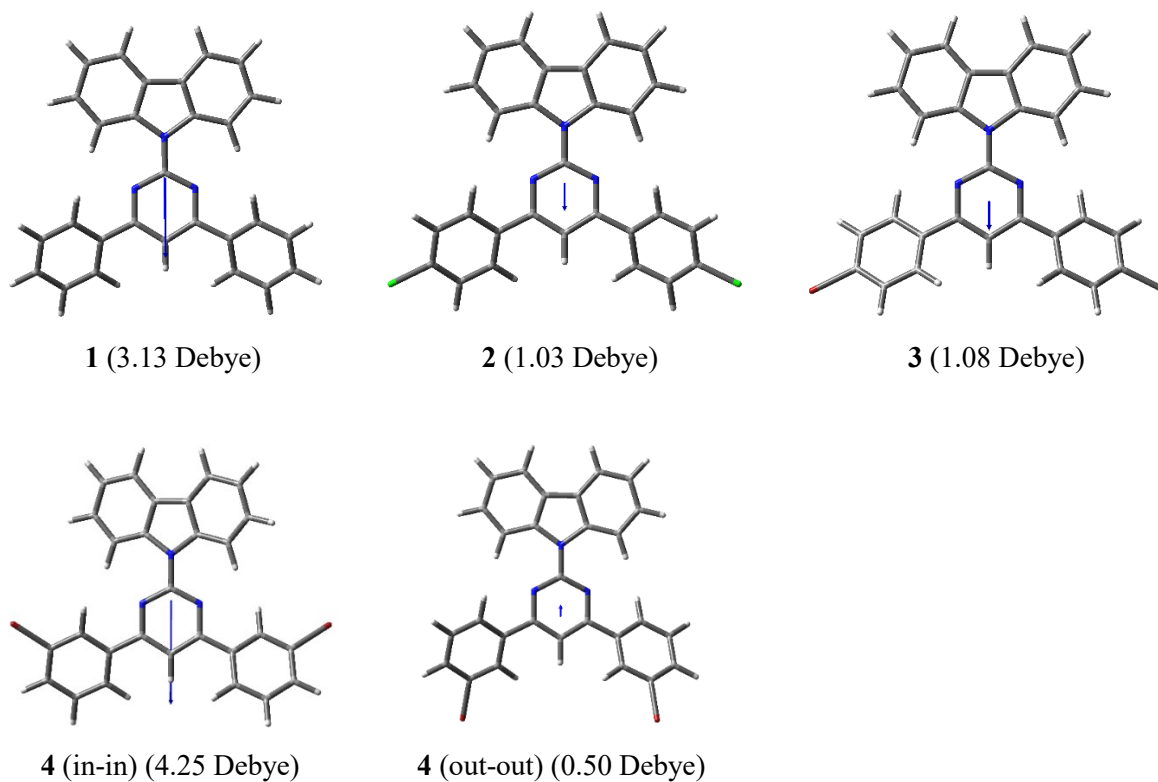


Fig. S26 The calculated molecular structures of **1**, **2**, **3**, **4** (in-in) and **4** (out-out) together with dipole moment (blue arrow) at the ground state. The structures were calculated as a monomer based on single crystal X-ray structures.

Table S6 Cartesian Coordinate of **1** at the M06-2X/6-31G(d) Level

Center Number	Atomic Number	Atomic Type	Coordinates (Angstroms)		
			X	Y	Z
1	7	0	0.393561	1.187427	-0.068107
2	7	0	0.393849	-1.187351	-0.068165
3	7	0	-1.603596	-0.000189	-0.130826
4	6	0	-0.211787	-0.000050	-0.088385
5	6	0	1.728827	1.188881	-0.032861
6	6	0	2.458347	0.000279	-0.016453
7	6	0	1.729154	-1.188497	-0.032932
8	6	0	-2.434093	-1.148353	-0.102062
9	6	0	-2.129805	-2.511591	-0.168934
10	6	0	-3.185031	-3.416719	-0.122804
11	6	0	-4.516003	-3.001133	-0.017026
12	6	0	-4.816057	-1.647777	0.031118
13	6	0	-3.773969	-0.723996	-0.016155
14	6	0	-3.774126	0.723166	-0.016295
15	6	0	-4.816462	1.646682	0.030772
16	6	0	-4.516751	3.000101	-0.017597
17	6	0	-3.185876	3.415987	-0.123386
18	6	0	-2.130418	2.511116	-0.169326
19	6	0	-2.434346	1.147807	-0.102248
20	6	0	2.391326	2.515412	0.025989
21	6	0	1.726221	3.594651	0.616422
22	6	0	2.339966	4.839036	0.693149
23	6	0	3.619508	5.021767	0.172303
24	6	0	4.283752	3.953608	-0.425342
25	6	0	3.674382	2.705425	-0.494922
26	6	0	2.391977	-2.514884	0.025828
27	6	0	3.675038	-2.704542	-0.495182
28	6	0	4.284728	-3.952572	-0.425730
29	6	0	3.620836	-5.020928	0.171939
30	6	0	2.341312	-4.838547	0.692942
31	6	0	1.727227	-3.594314	0.616317
32	1	0	3.536269	0.000441	0.083115
33	1	0	-1.112333	-2.853926	-0.267995
34	1	0	-2.960044	-4.477667	-0.176051
35	1	0	-5.312561	-3.737456	0.018796
36	1	0	-5.844926	-1.306025	0.099013
37	1	0	-5.845233	1.304646	0.098703
38	1	0	-5.313480	3.736245	0.018045
39	1	0	-2.961145	4.476983	-0.176786
40	1	0	-1.113035	2.853731	-0.268360
41	1	0	0.733717	3.438093	1.027126
42	1	0	1.820894	5.667991	1.164105
43	1	0	4.096763	5.995202	0.230532
44	1	0	5.275340	4.093465	-0.844263
45	1	0	4.186741	1.881676	-0.983640
46	1	0	4.187116	-1.880643	-0.983939
47	1	0	5.276304	-4.092162	-0.844767
48	1	0	4.098371	-5.994229	0.230085
49	1	0	1.822513	-5.667634	1.163968
50	1	0	0.734750	-3.438041	1.027171

No imaginary frequency.

Total energy: -1242.22432143 hartree.

Table S7 Cartesian Coordinate of **2** at the M06-2X/6-31G(d) Level

Center Number	Atomic Number	Atomic Type	Coordinates (Angstroms)		
			X	Y	Z
1	17	0	-6.570464	-3.790911	0.196046
2	17	0	6.571297	-3.789712	0.195755
3	7	0	-0.000221	2.188412	-0.154198
4	7	0	-1.187327	0.190737	-0.115353
5	7	0	1.187364	0.191024	-0.115621
6	6	0	-1.187470	-1.144049	-0.094597
7	6	0	-2.513951	-1.805629	-0.039969
8	6	0	-3.952035	-3.701533	-0.497267
9	6	0	2.514462	-1.805061	-0.040198
10	6	0	1.187837	-1.143781	-0.094680
11	6	0	1.148467	3.019217	-0.106636
12	6	0	0.723166	4.355658	0.014314
13	6	0	2.999582	5.099232	0.027381
14	6	0	-0.724328	4.355435	0.014114
15	6	0	5.009977	-3.024022	0.101627
16	6	0	-2.511901	2.717184	-0.187440
17	6	0	-1.647531	5.396465	0.086062
18	6	0	4.842155	-1.746048	0.626898
19	6	0	-0.000049	0.798548	-0.129127
20	6	0	-2.707153	-3.087538	-0.561327
21	6	0	-5.009225	-3.025015	0.101928
22	6	0	-3.417018	3.771275	-0.116460
23	6	0	-1.149204	3.018882	-0.106924
24	6	0	-3.000934	5.098430	0.026373
25	6	0	0.000285	-1.875102	-0.086333
26	6	0	1.646074	5.396910	0.086626
27	6	0	2.511272	2.717879	-0.186728
28	6	0	3.595073	-1.140882	0.548434
29	6	0	3.952997	-3.700519	-0.497983
30	6	0	3.416091	3.772211	-0.115375
31	6	0	2.707994	-3.086739	-0.562006
32	6	0	-3.594767	-1.141441	0.548287
33	6	0	-4.841742	-1.746815	0.626787
34	1	0	-4.107594	-4.691129	-0.912325
35	1	0	3.735400	5.895037	0.082403
36	1	0	-2.854813	1.703461	-0.317137
37	1	0	-1.305485	6.422986	0.181288
38	1	0	5.679177	-1.239531	1.094742
39	1	0	-1.886998	-3.604754	-1.050225
40	1	0	-4.477822	3.548700	-0.180435
41	1	0	-3.737008	5.894011	0.081112
42	1	0	0.000357	-2.953804	0.004322
43	1	0	1.303753	6.423346	0.181751
44	1	0	2.854436	1.704255	-0.316457
45	1	0	3.442170	-0.148760	0.960840
46	1	0	4.108841	-4.689899	-0.913443
47	1	0	4.476982	3.549954	-0.178995
48	1	0	1.888052	-3.603975	-1.051204
49	1	0	-3.442111	-0.149109	0.960320
50	1	0	-5.678953	-1.240335	1.094343

No imaginary frequency.

Total energy: -2161.36405998 hartree.

Table S8 Cartesian Coordinate of **3** at the M06-2X/6-31G(d) Level

Center Number	Atomic Number	Atomic Type	Coordinates (Angstroms)		
			X	Y	Z
1	35	0	6.686703	-3.356299	-0.205997
2	35	0	-6.686291	-3.356831	-0.206405
3	7	0	-0.000108	2.707115	0.191203
4	7	0	1.187244	0.709317	0.196053
5	7	0	-1.187153	0.709159	0.195839
6	6	0	-5.001325	-2.515708	-0.049155
7	6	0	-0.000001	1.317103	0.198581
8	6	0	-1.187467	-0.625756	0.199386
9	6	0	-0.724167	4.866940	-0.052859
10	6	0	1.148641	3.535849	0.114720
11	6	0	1.187684	-0.625596	0.199504
12	6	0	4.827470	-1.239110	-0.575118
13	6	0	5.001674	-2.515296	-0.048837
14	6	0	2.514049	-1.287246	0.139198
15	6	0	-2.513783	-1.287519	0.138996
16	6	0	-2.511653	3.236874	0.207557
17	6	0	3.957200	-3.183474	0.580453
18	6	0	-1.149086	3.535603	0.115330
19	6	0	0.723344	4.867100	-0.053259
20	6	0	2.511331	3.237408	0.206137
21	6	0	1.646251	5.905129	-0.163035
22	6	0	0.000159	-1.357137	0.208237
23	6	0	-3.416819	4.287747	0.098810
24	6	0	2.715205	-2.565284	0.667221
25	6	0	-3.956750	-3.183982	0.579859
26	6	0	-2.714797	-2.565718	0.666683
27	6	0	3.416212	4.288463	0.096808
28	6	0	2.999682	5.609561	-0.093522
29	6	0	-3.000678	5.608939	-0.091735
30	6	0	-3.584561	-0.628790	-0.473499
31	6	0	-4.827281	-1.239366	-0.575099
32	6	0	3.584714	-0.628597	-0.473571
33	6	0	-1.647349	5.904786	-0.162055
34	1	0	5.654969	-0.737824	-1.064250
35	1	0	-2.854224	2.228320	0.373980
36	1	0	4.117314	-4.171158	0.997781
37	1	0	2.854189	2.228933	0.372414
38	1	0	1.303998	6.927513	-0.294903
39	1	0	0.000261	-2.437261	0.136071
40	1	0	-4.477624	4.067758	0.171229
41	1	0	1.903613	-3.077860	1.175109
42	1	0	-4.116761	-4.171788	0.996934
43	1	0	-1.903143	-3.078376	1.174395
44	1	0	4.477108	4.068705	0.168598
45	1	0	3.735737	6.402556	-0.177429
46	1	0	-3.736957	6.401772	-0.175184
47	1	0	-3.426222	0.361149	-0.889170
48	1	0	-5.654866	-0.738030	-1.064035
49	1	0	3.426293	0.361227	-0.889470
50	1	0	-1.305384	6.927241	-0.294103

No imaginary frequency.

Total energy: -6384.58850513 hartree.

Table S9 Cartesian Coordinate of **4**(in-in) at the M06-2X/6-31G(d) Level

Center Number	Atomic Number	Atomic Type	Coordinates (Angstroms)		
			X	Y	Z
1	35	0	6.438875	-0.960929	-0.553142
2	7	0	-0.000002	1.900815	-0.000012
3	7	0	1.184625	-0.093765	0.075420
4	6	0	1.077466	2.728456	0.395689
5	6	0	-0.000000	0.512301	0.000011
6	6	0	0.678653	4.070838	0.253110
7	6	0	2.340117	2.410885	0.902473
8	6	0	1.185189	-1.428141	0.094680
9	6	0	2.516006	-2.082032	0.201167
10	6	0	3.654870	-1.354569	-0.158998
11	6	0	0.000003	-2.158102	0.000081
12	6	0	3.185862	3.462247	1.239620
13	6	0	4.903217	-1.950959	-0.063762
14	6	0	2.655424	-3.394126	0.661374
15	6	0	5.051782	-3.258415	0.387756
16	6	0	3.915837	-3.974510	0.752276
17	6	0	2.803223	4.799001	1.085053
18	6	0	1.543729	5.109146	0.593629
19	35	0	-6.438896	-0.960904	0.553050
20	7	0	-1.184624	-0.093772	-0.075368
21	6	0	-1.077468	2.728442	-0.395748
22	6	0	-0.678650	4.070829	-0.253226
23	6	0	-2.340123	2.410856	-0.902514
24	6	0	-1.185184	-1.428149	-0.094558
25	6	0	-2.515996	-2.082051	-0.201032
26	6	0	-3.654873	-1.354568	0.159051
27	6	0	-3.185864	3.462207	-1.239701
28	6	0	-4.903214	-1.950969	0.063814
29	6	0	-2.655394	-3.394177	-0.661156
30	6	0	-5.051760	-3.258456	-0.387621
31	6	0	-3.915800	-3.974572	-0.752056
32	6	0	-2.803220	4.798966	-1.085192
33	6	0	-1.543724	5.109127	-0.593785
34	1	0	2.654750	1.386169	1.029572
35	1	0	3.551591	-0.335792	-0.515467
36	1	0	0.000004	-3.239621	0.000103
37	1	0	4.171452	3.230592	1.631736
38	1	0	1.784241	-3.958342	0.978130
39	1	0	6.039360	-3.700514	0.457600
40	1	0	4.019147	-4.990237	1.120052
41	1	0	3.492293	5.592926	1.354428
42	1	0	1.228621	6.142259	0.478531
43	1	0	-2.654762	1.386136	-1.029565
44	1	0	-3.551609	-0.335763	0.515445
45	1	0	-4.171458	3.230540	-1.631803
46	1	0	-1.784197	-3.958408	-0.977848
47	1	0	-6.039335	-3.700562	-0.457471
48	1	0	-4.019095	-4.990323	-1.119769
49	1	0	-3.492288	5.592883	-1.354599
50	1	0	-1.228611	6.142243	-0.478731

No imaginary frequency.

Total energy: -6384.58861874 hartree.

Table S10 Cartesian Coordinate of 4(out-out) at the M06-2X/6-31G(d) Level

Center Number	Atomic Number	Atomic Type	Coordinates (Angstroms)		
			X	Y	Z
1	35	0	-4.521004	4.258749	-0.587270
2	7	0	3.088968	-0.000209	0.000041
3	7	0	1.094039	1.168838	0.211582
4	6	0	3.917096	1.143387	-0.097052
5	6	0	1.699402	-0.000185	0.000087
6	6	0	5.259800	0.721047	-0.064780
7	6	0	3.600084	2.496089	-0.248145
8	6	0	-0.240368	1.173329	0.188309
9	6	0	-0.900886	2.488402	0.391605
10	6	0	-2.188159	2.719823	-0.098553
11	6	0	-0.969893	-0.000022	0.000030
12	6	0	4.652126	3.400111	-0.348349
13	6	0	-2.784742	3.957332	0.101611
14	6	0	-0.228176	3.508619	1.071329
15	6	0	-2.129747	4.974676	0.785657
16	6	0	-0.845184	4.738524	1.269056
17	6	0	5.988919	2.990112	-0.301676
18	6	0	6.298625	1.645192	-0.162720
19	35	0	-4.521581	-4.258293	0.587193
20	7	0	1.093907	-1.169130	-0.211468
21	6	0	3.917184	-1.143759	0.097087
22	6	0	5.259859	-0.721312	0.064679
23	6	0	3.600315	-2.496492	0.248243
24	6	0	-0.240502	-1.173459	-0.188238
25	6	0	-0.901177	-2.488452	-0.391540
26	6	0	-2.188500	-2.719696	0.098570
27	6	0	4.652448	-3.400420	0.348354
28	6	0	-2.785238	-3.957128	-0.101597
29	6	0	-0.228575	-3.508767	-1.071224
30	6	0	-2.130350	-4.974572	-0.785598
31	6	0	-0.845736	-4.738596	-1.268951
32	6	0	5.989201	-2.990311	0.301532
33	6	0	6.298773	-1.645368	0.162525
34	1	0	2.575110	2.832434	-0.284964
35	1	0	-2.720154	1.959033	-0.659120
36	1	0	-2.051708	0.000041	0.000021
37	1	0	4.421798	4.454603	-0.466201
38	1	0	0.772345	3.318907	1.445771
39	1	0	-2.616265	5.932711	0.930747
40	1	0	-0.324617	5.525502	1.805199
41	1	0	6.782629	3.726027	-0.380283
42	1	0	7.331651	1.310591	-0.135693
43	1	0	2.575383	-2.832937	0.285180
44	1	0	-2.720419	-1.958823	0.659099
45	1	0	4.422224	-4.454930	0.466251
46	1	0	0.771983	-3.319192	-1.445634
47	1	0	-2.616990	-5.932542	-0.930696
48	1	0	-0.325253	-5.525651	-1.805061
49	1	0	6.782982	-3.726156	0.380071
50	1	0	7.331768	-1.310678	0.135393

No imaginary frequency.

Total energy: -6384.58888367 hartree.

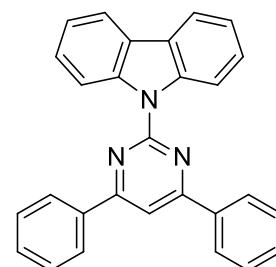
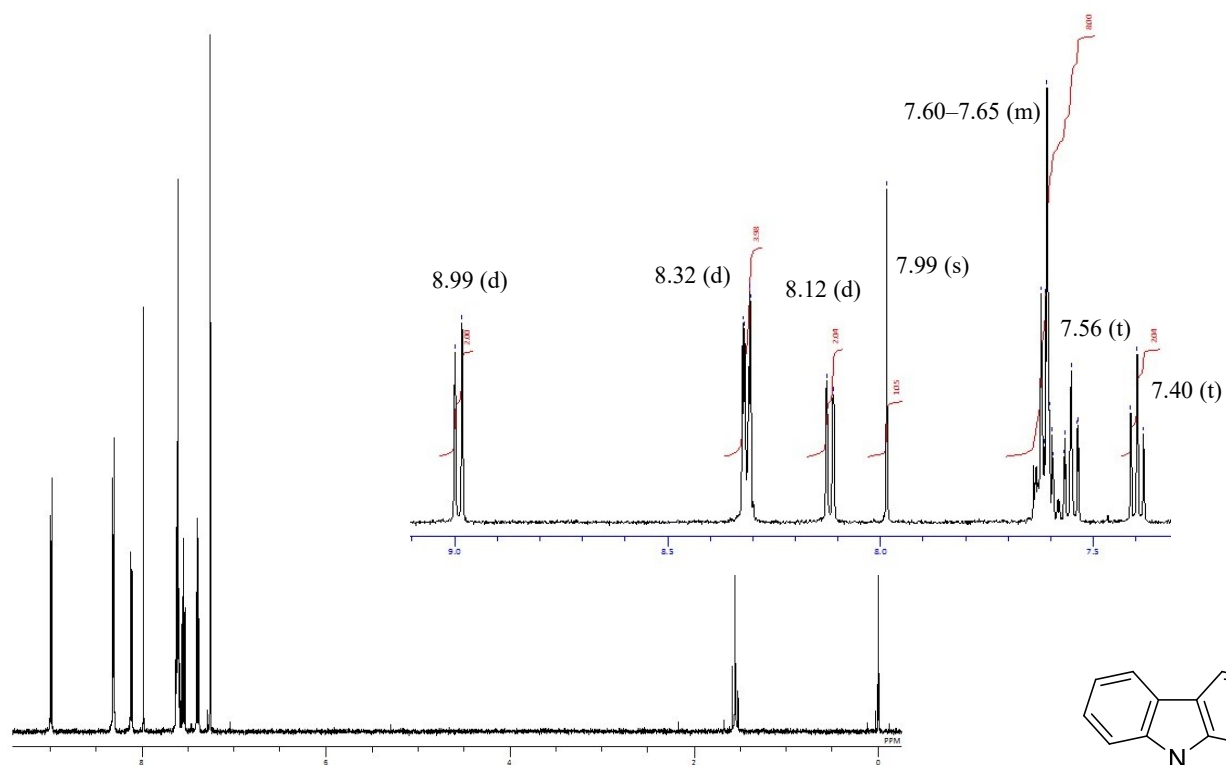


Fig. S27 ^1H NMR spectrum of **1** in CDCl_3 .

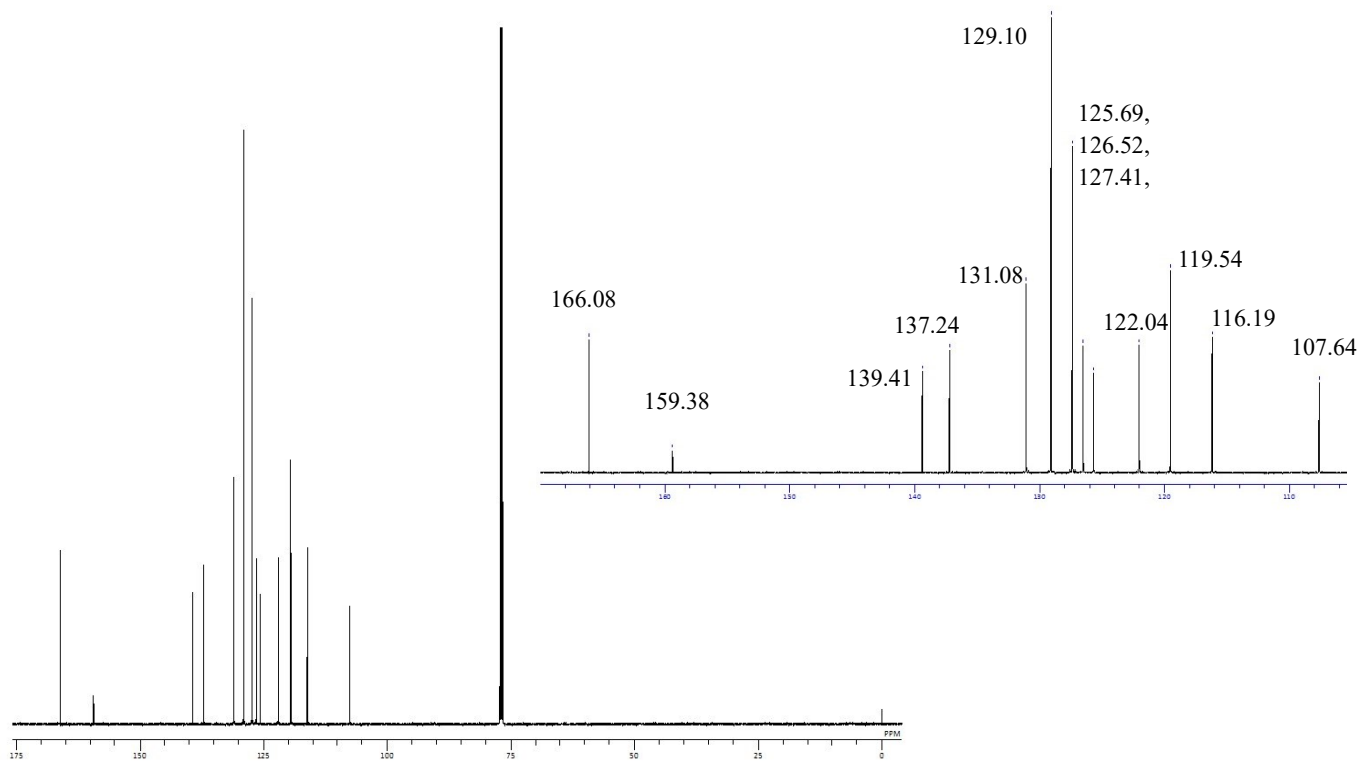


Fig. S28 ^{13}C NMR spectrum of **1** in CDCl_3 .

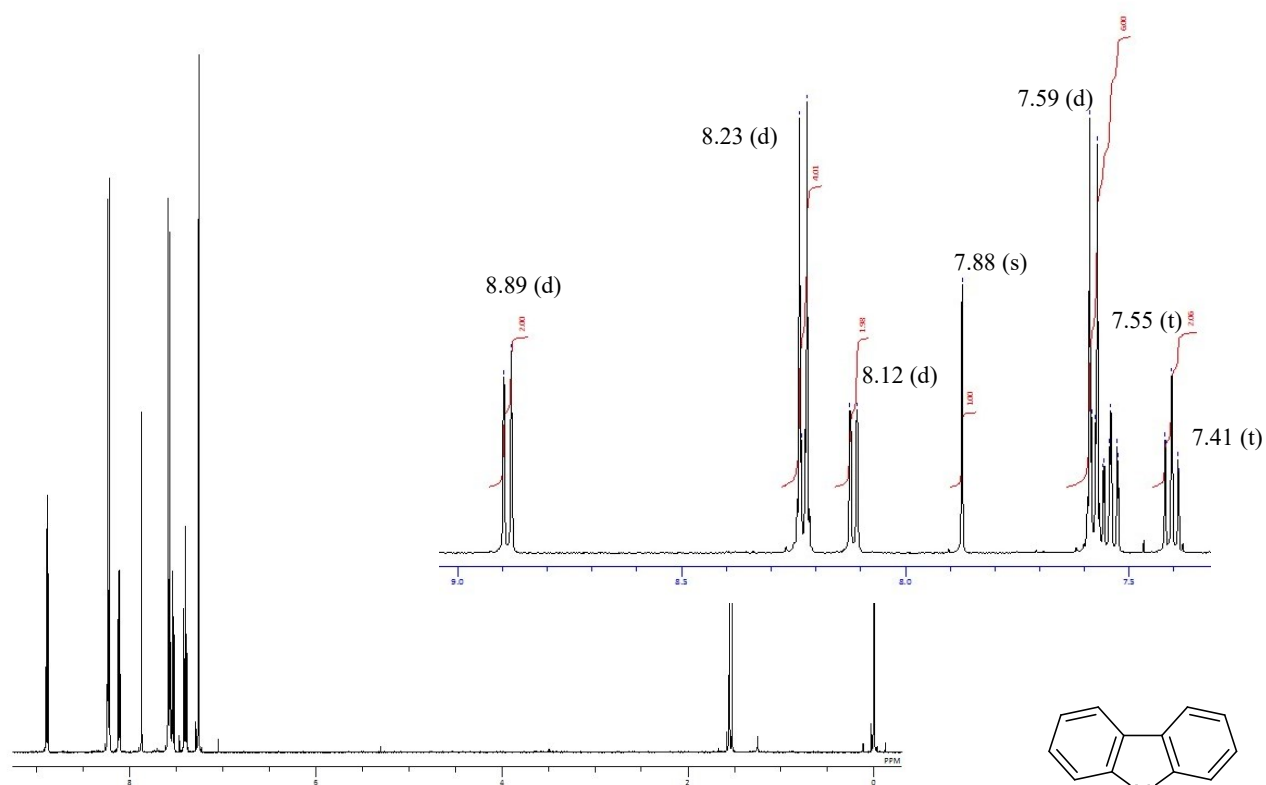


Fig. S29 ^1H NMR spectrum of **2** in CDCl_3 .

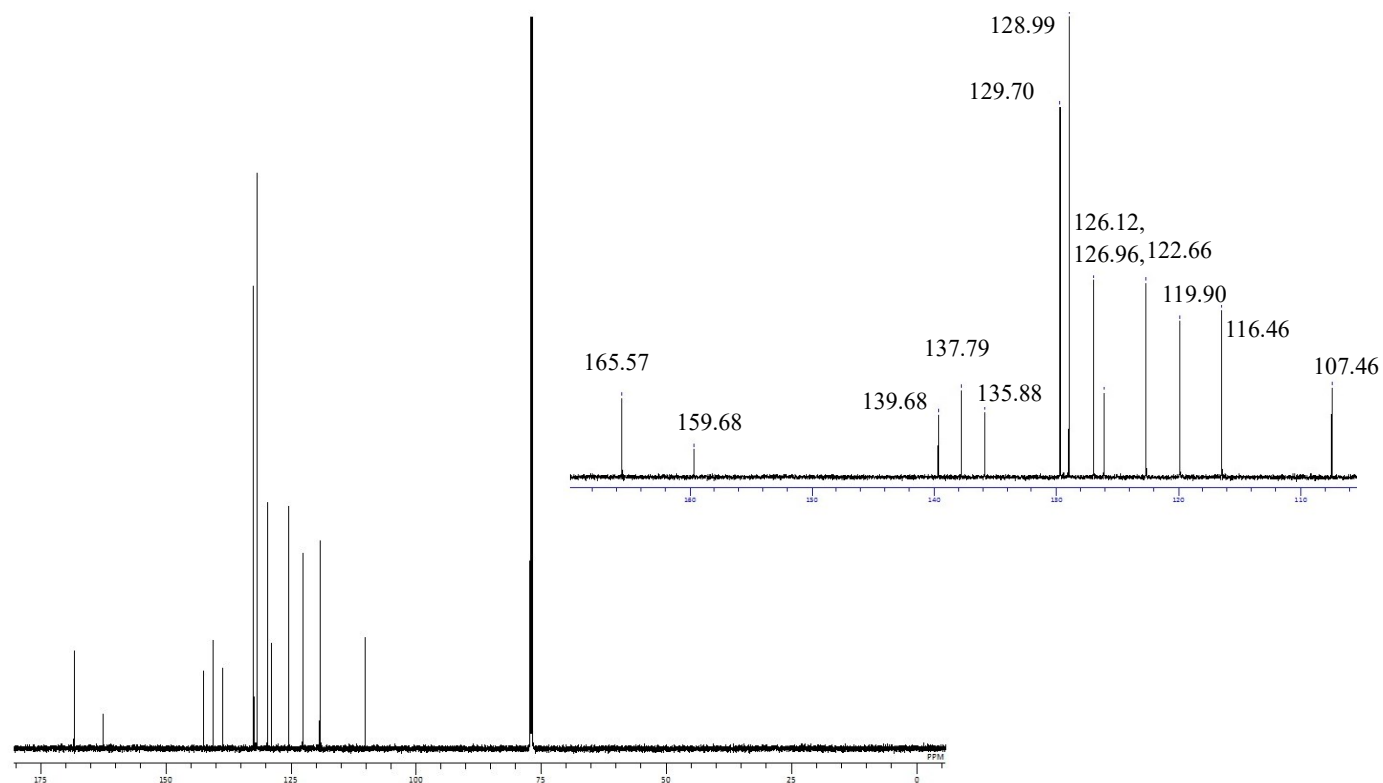
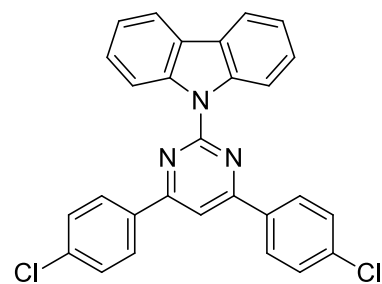


Fig. S30 ^{13}C NMR spectrum of **2** in $\text{CDCl}_2\text{CDCl}_2$.

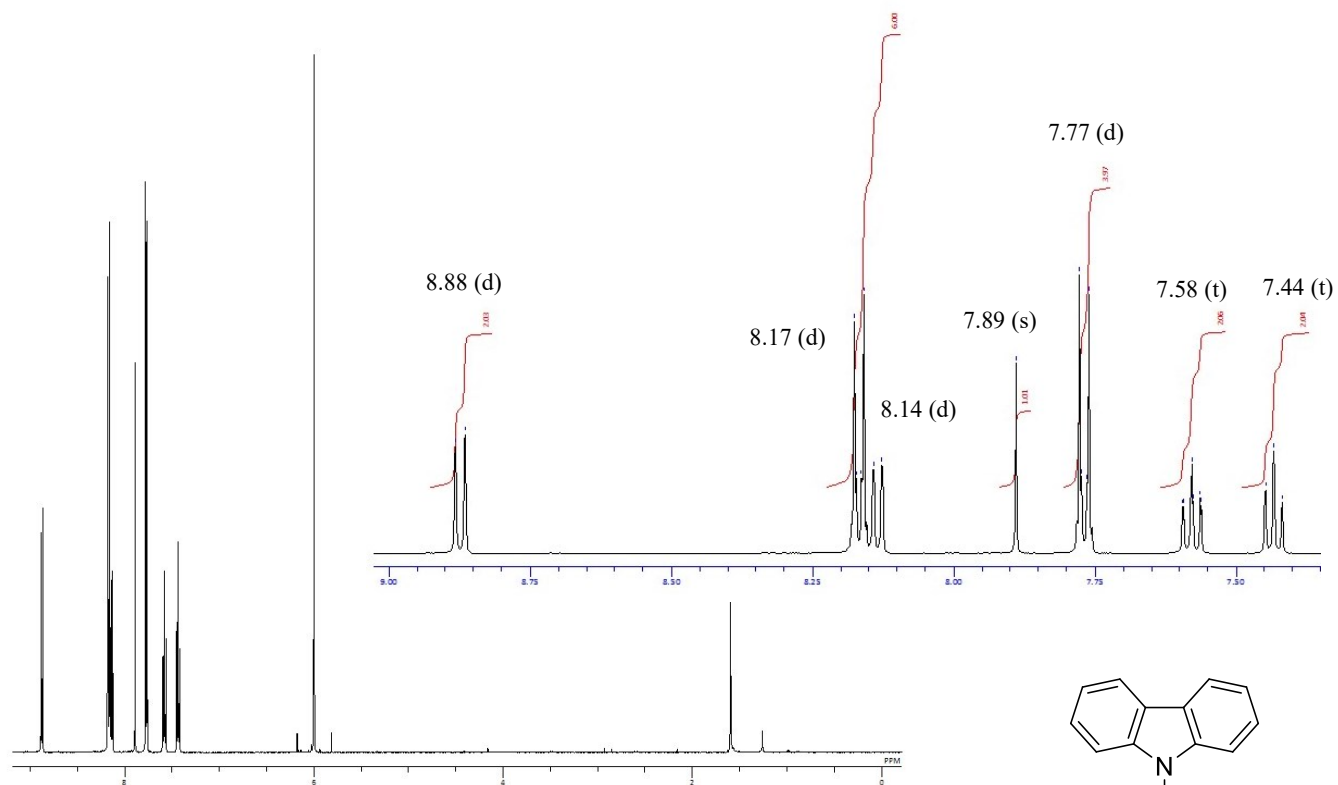


Fig. S31 ^1H NMR spectrum of **3** in $\text{CDCl}_2/\text{CDCl}_2$.

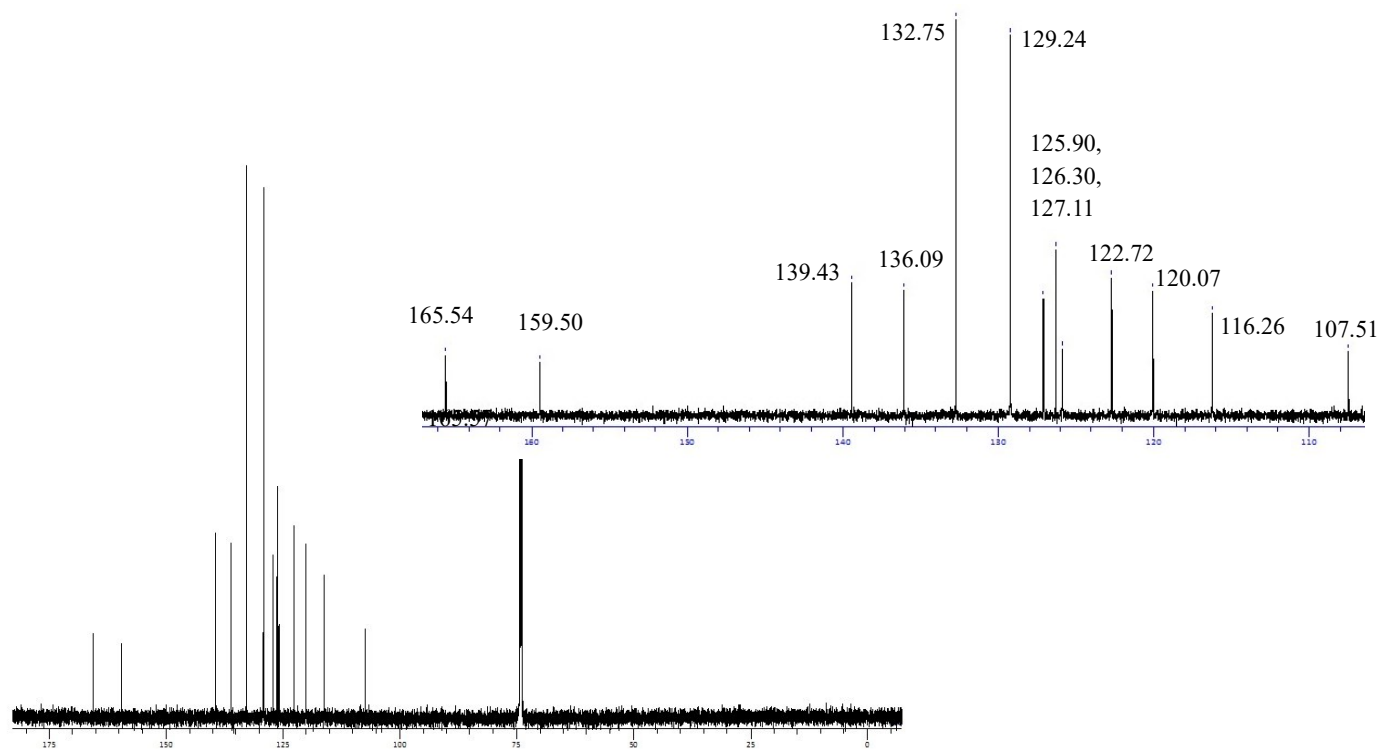
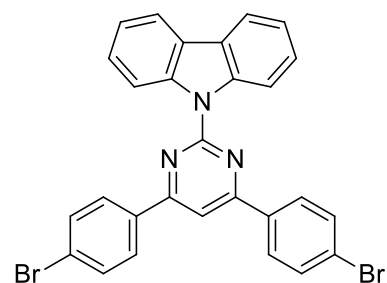
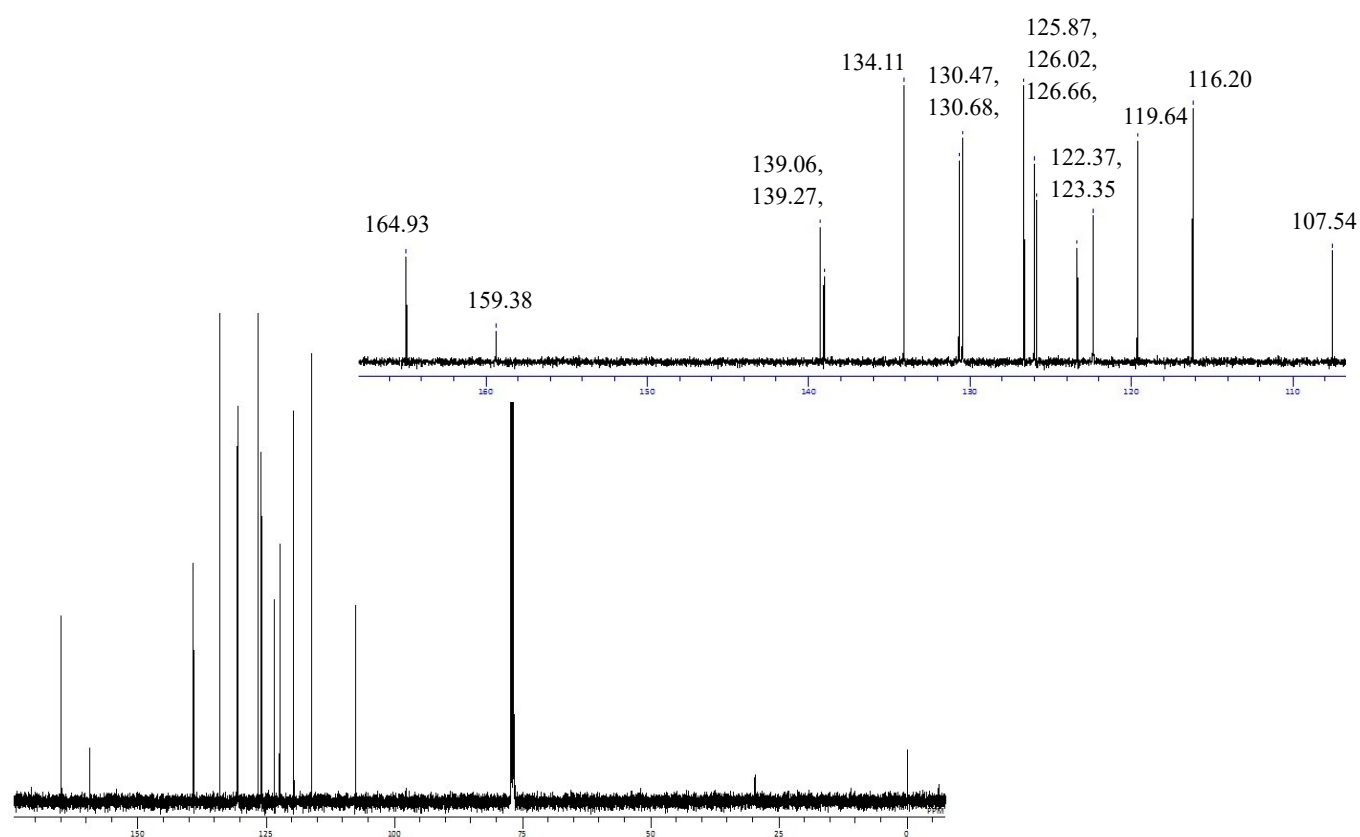
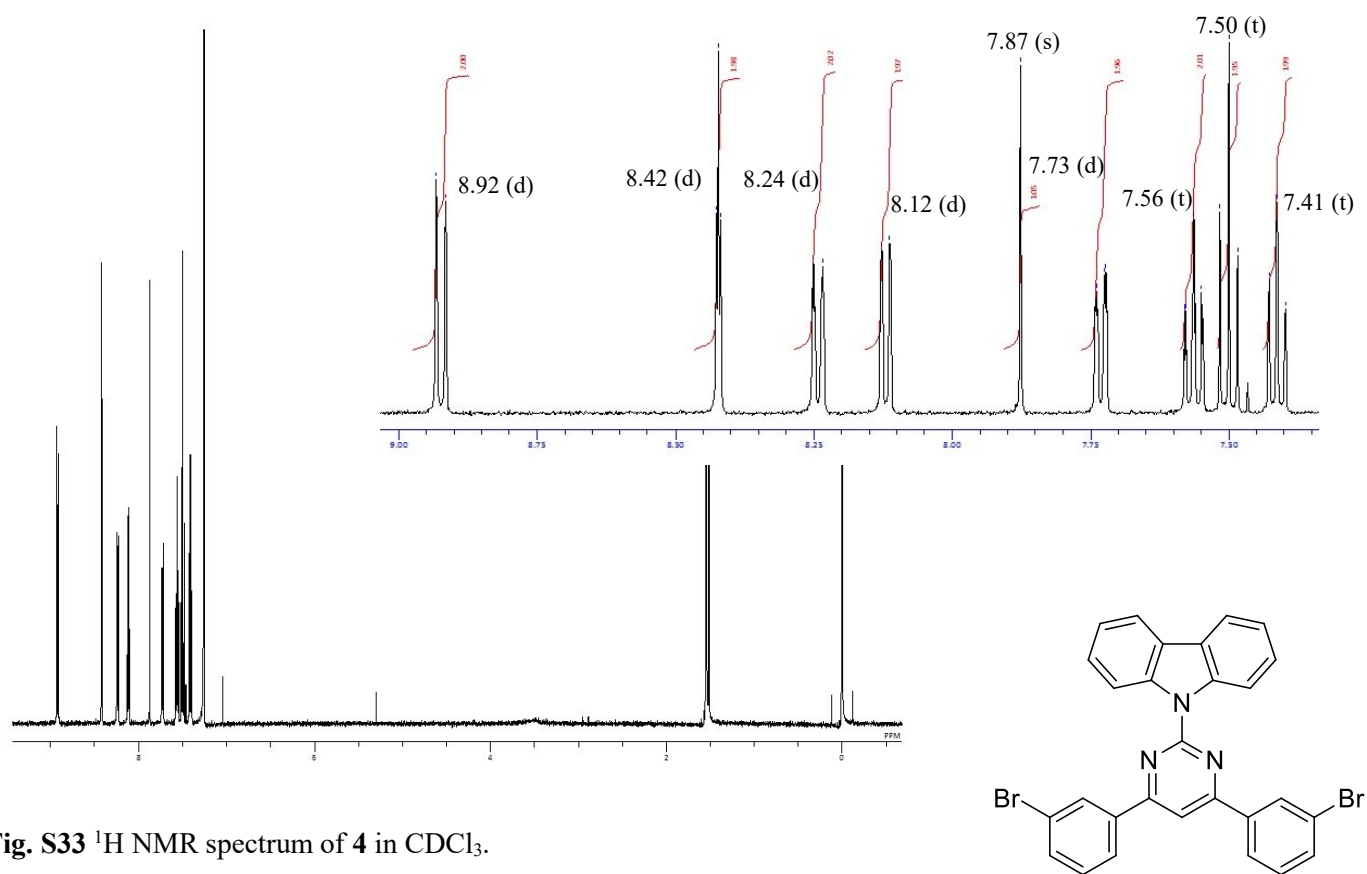


Fig. S32 ^{13}C NMR spectrum of **3** in $\text{CDCl}_2/\text{CDCl}_2$.



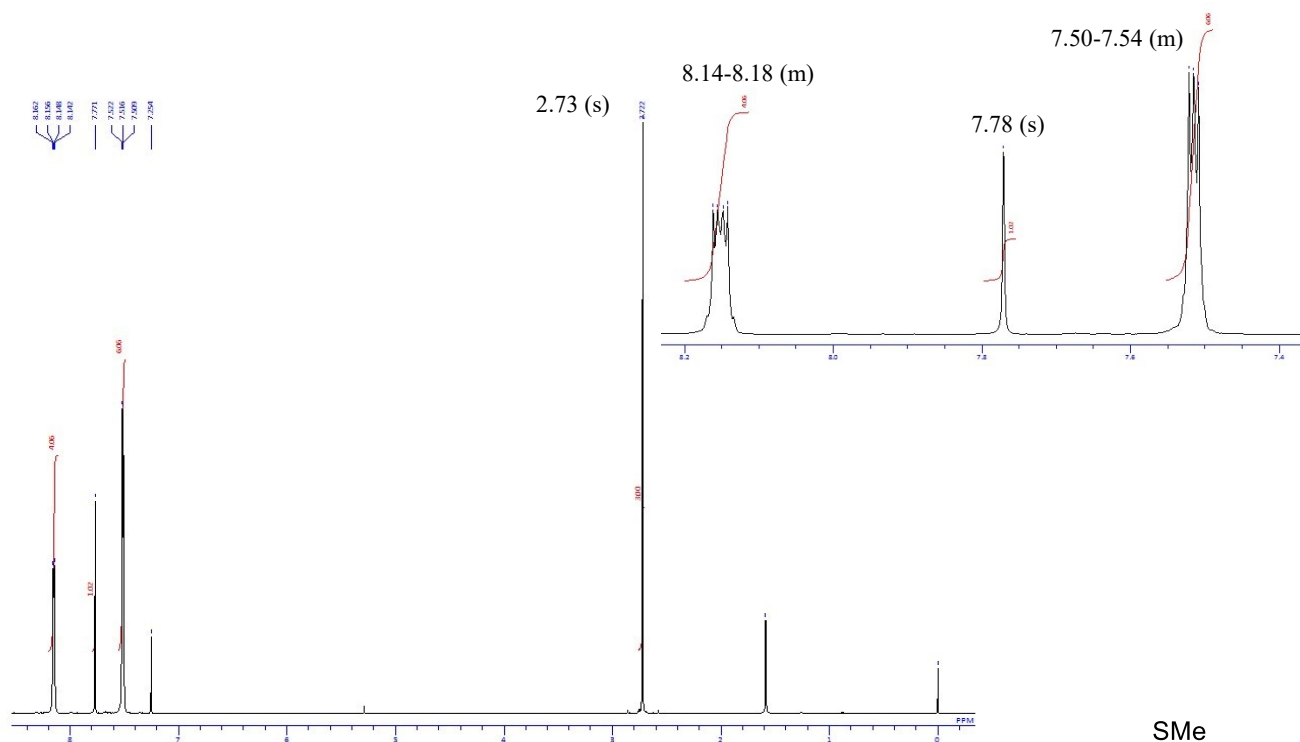


Fig. S35 ¹H NMR spectrum of 6a in CDCl₃.

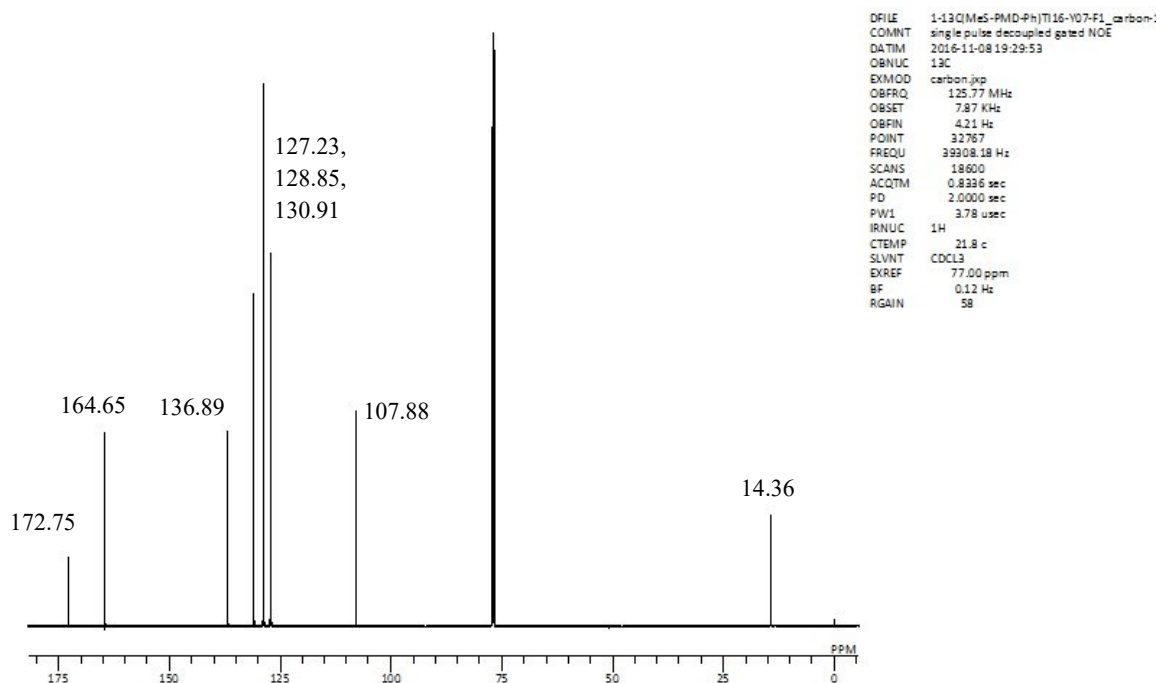


Fig. S36 ¹³C NMR spectrum of 6a in CDCl₃.

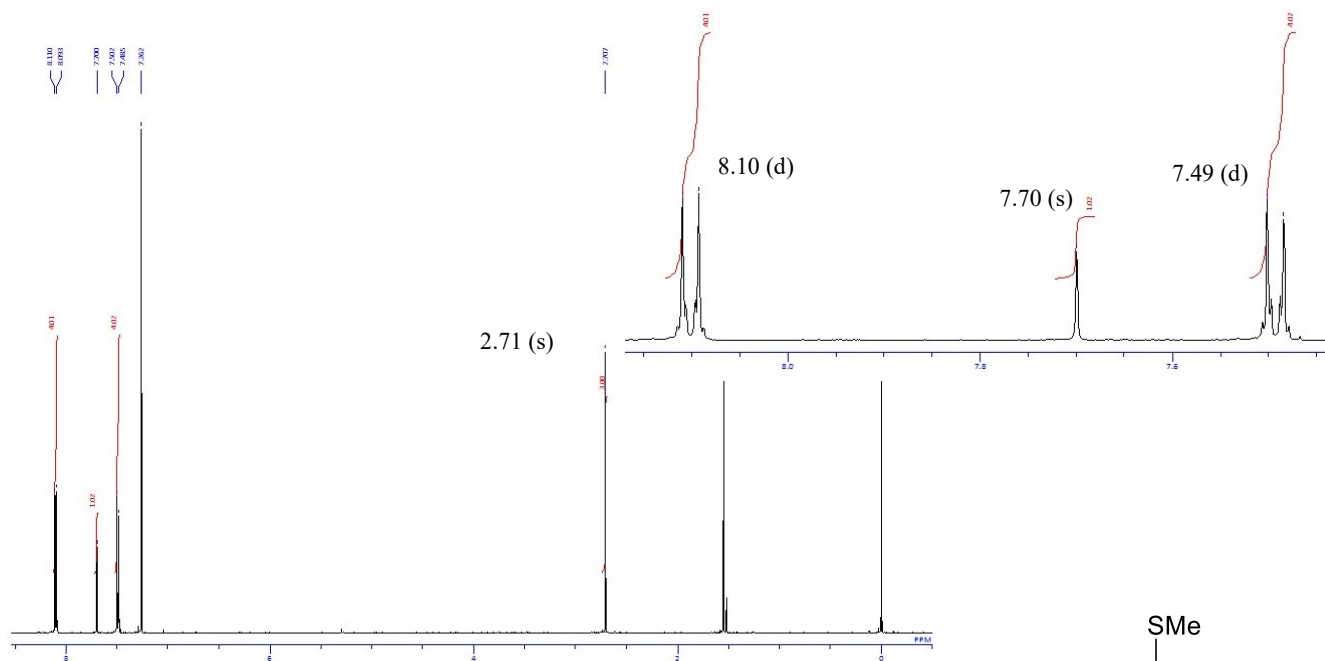


Fig. S37 ^1H NMR spectrum of **6b** in CDCl_3 .

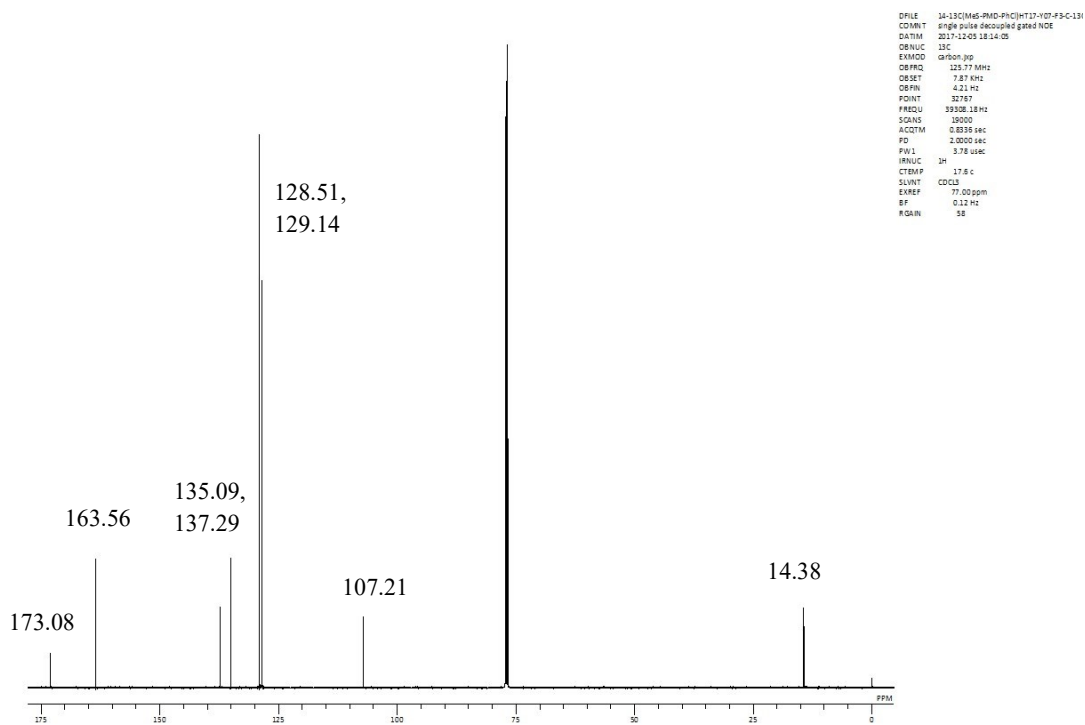


Fig. S38 ^{13}C NMR spectrum of **6b** in CDCl_3 .

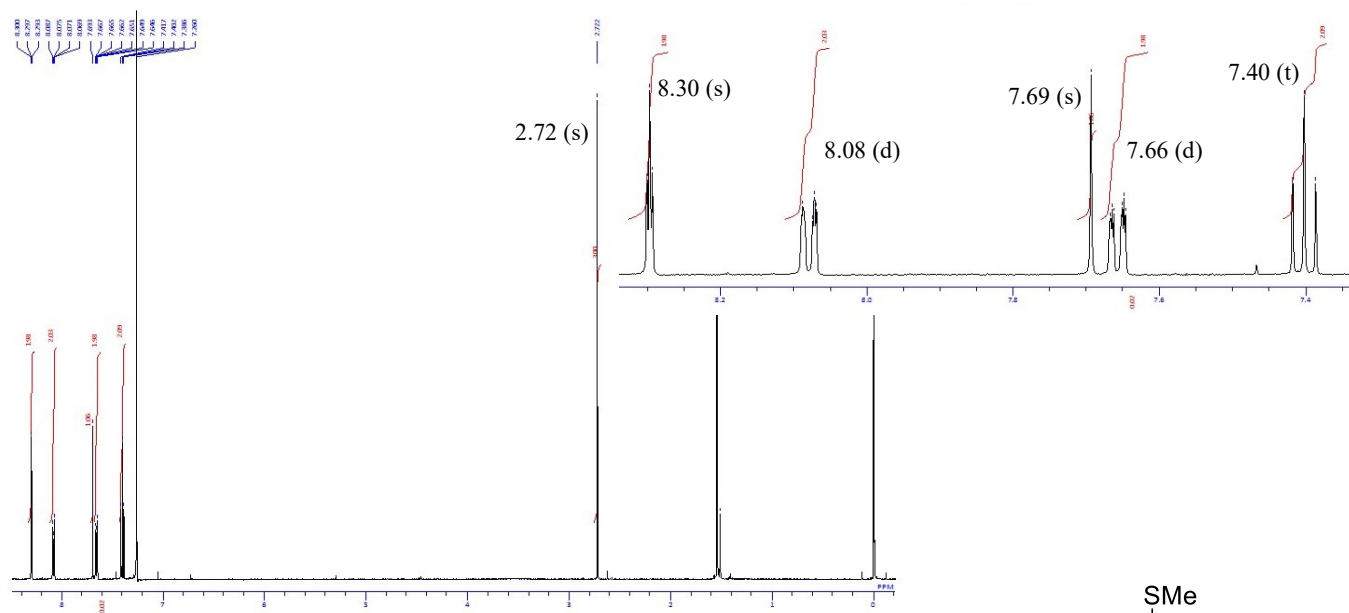


Fig. S41 ¹H NMR spectrum of **6d** in CDCl₃.

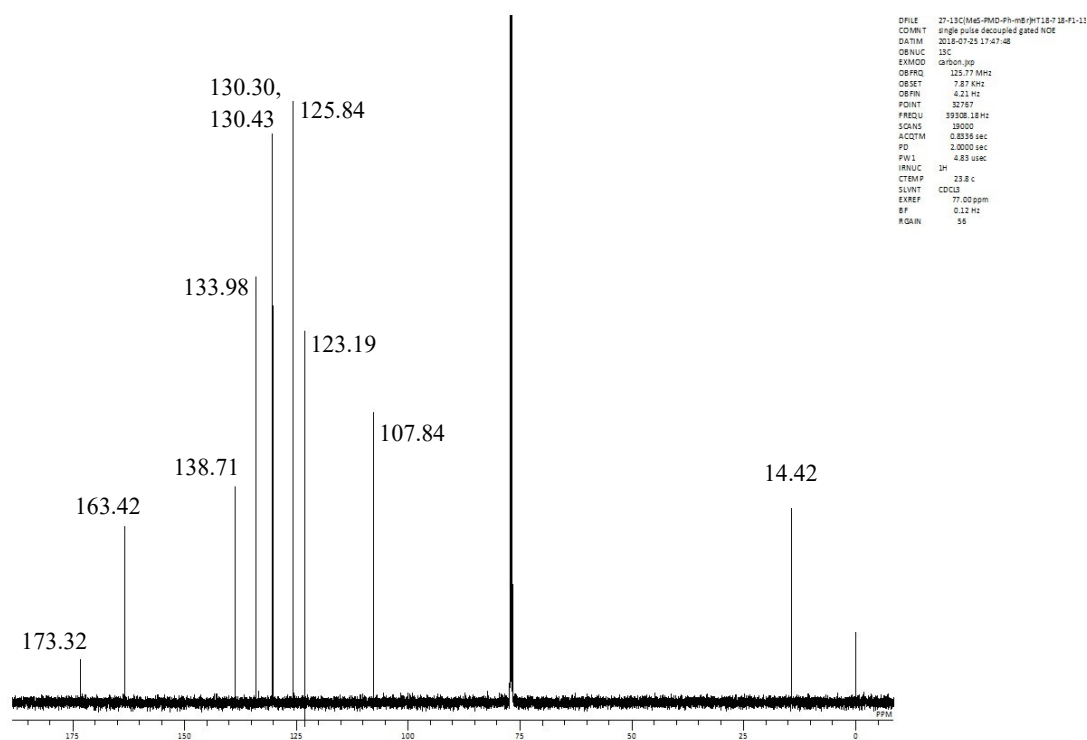
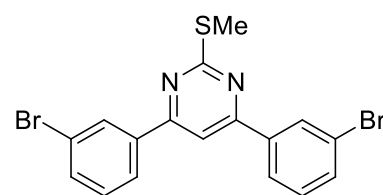


Fig. S42 ¹³C NMR spectrum of **6d** in CDCl₃.

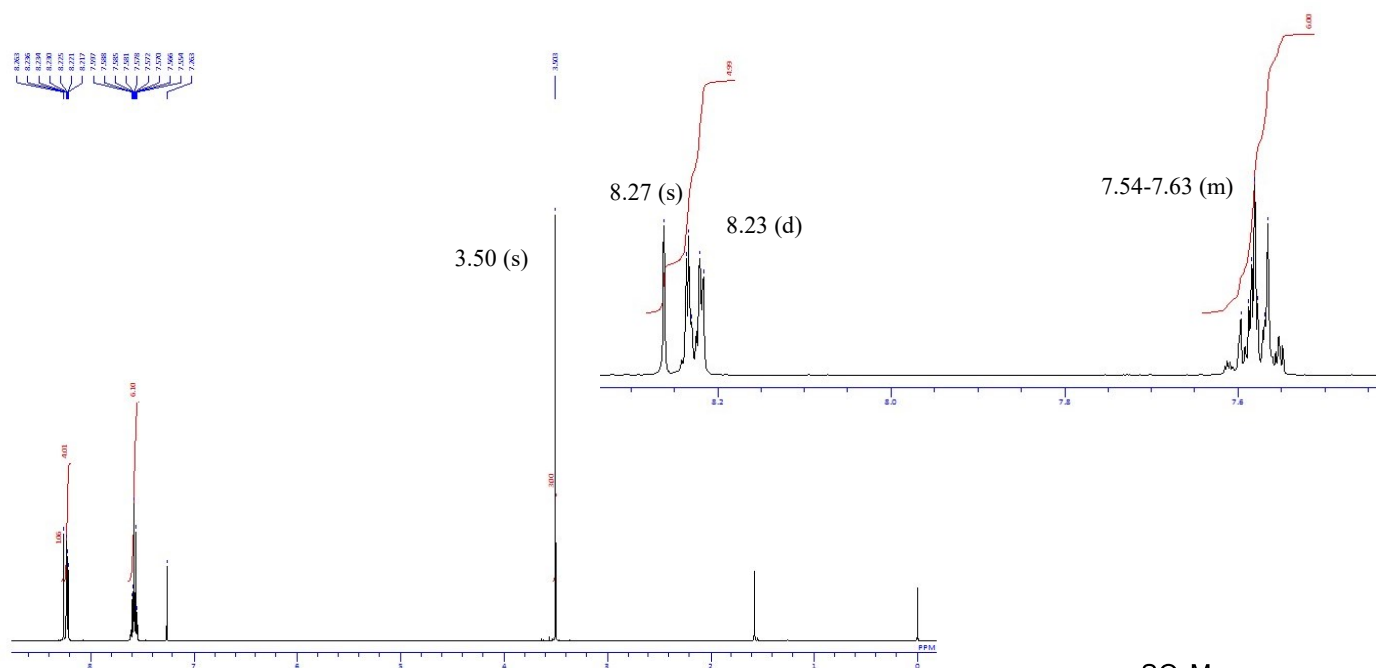


Fig. S43 ¹H NMR spectrum of **7a** in CDCl₃.

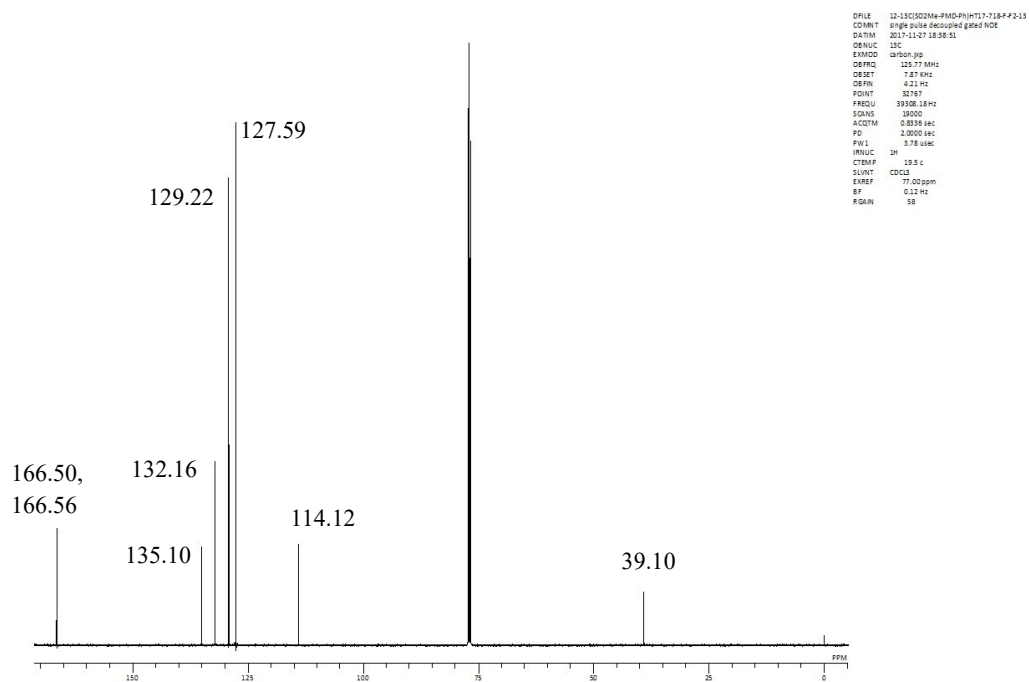
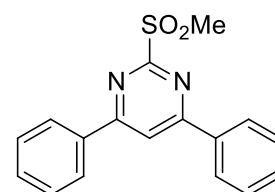


Fig. S44 ¹³C NMR spectrum of **7a** in CDCl₃.

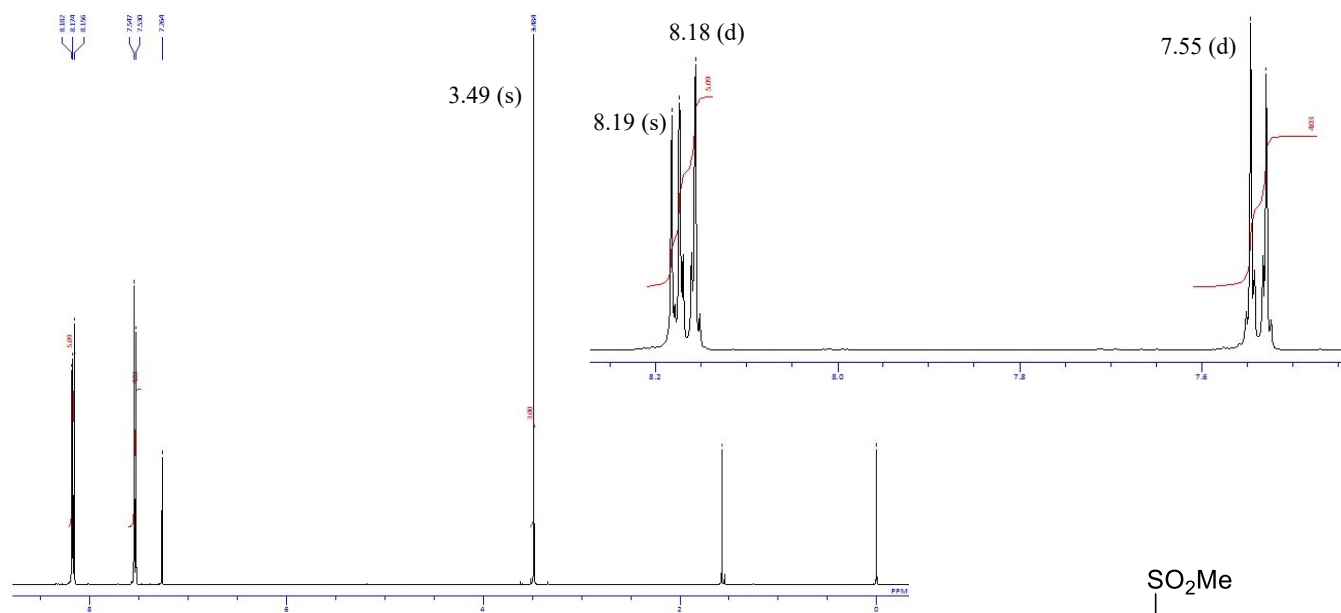
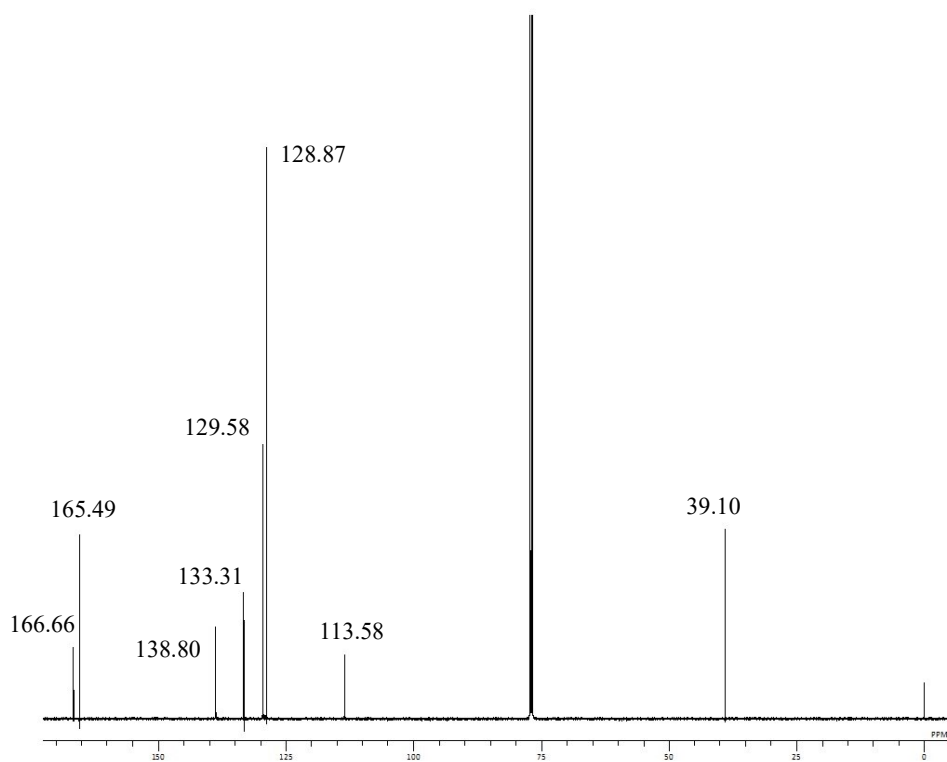
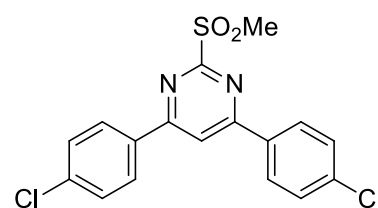


Fig. S45 ¹H NMR spectrum of **7b** in CDCl₃.



```

D:FILE 15-13(SO2Me-PMD-PHCl)HTL7-120-C-1
COMNT single pulse decoupled gated NDE
D:TIME 2017-11-28 19:25:29
SFC
OBNUC carbon.jpg
EXMODO
DEPMQ 125.77 MHz
OBSET 7.87 KHz
OBFM 4.21 Hz
POINT 32767
FREQU 399.9818 Hz
SCANS 19403
AQTM 0.0000 sec
FO 3.0000 sec
PW1 3.78 usec
INUC 1H
CTEMP 21.4 c
SLVNT CDCl3
EXREF 77.00 ppm
BF 0.12 Hz
RGAIN 58
  
```

Fig.S46 ¹³C NMR spectrum of **7b** in CDCl₃.

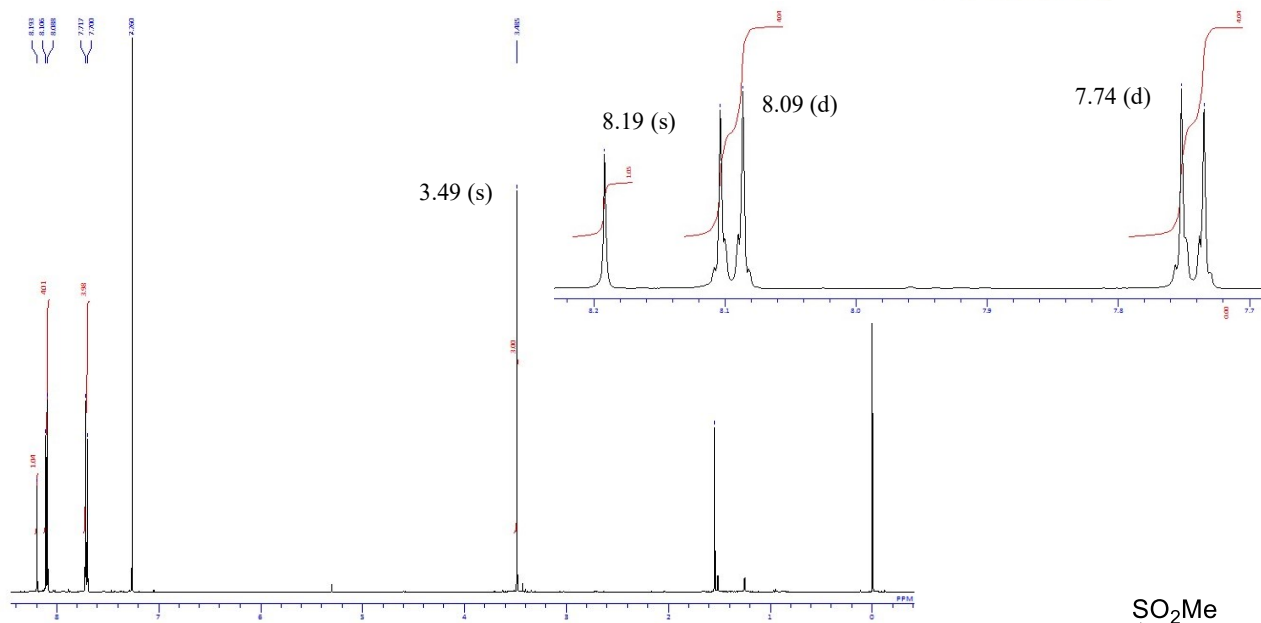


Fig. S47 ^1H NMR spectrum of **7c** in $\text{CDCl}_2/\text{CDCl}_2$.

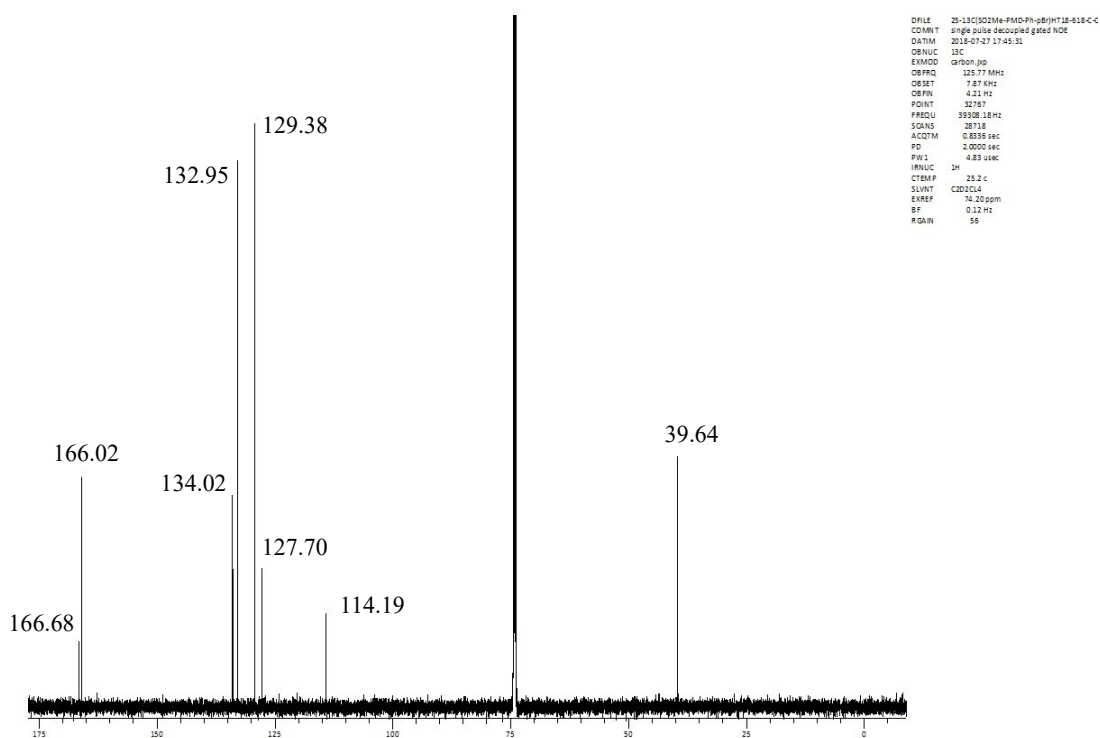
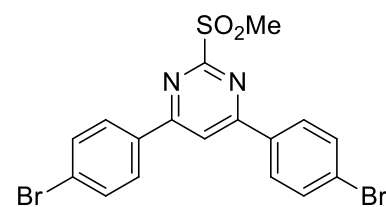


Fig. S48 ^{13}C NMR spectrum of **7c** in $\text{CDCl}_2/\text{CDCl}_2$.

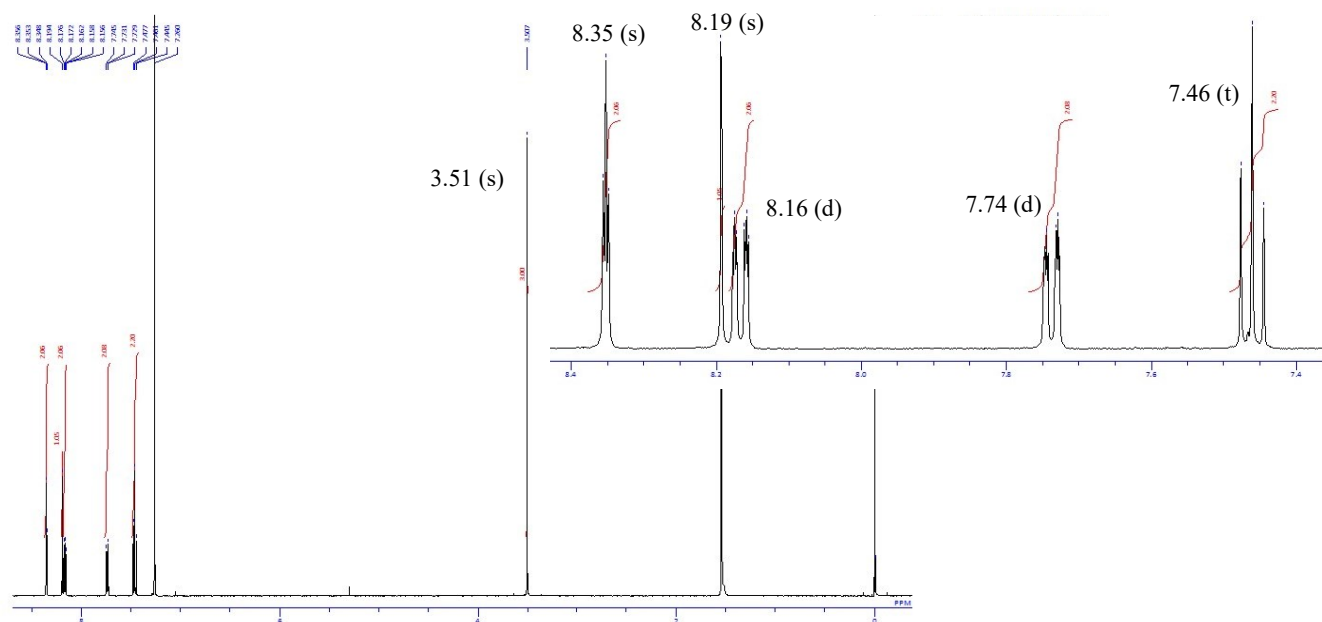


Fig. S49 ¹H NMR spectrum of **7d** in CDCl₃.

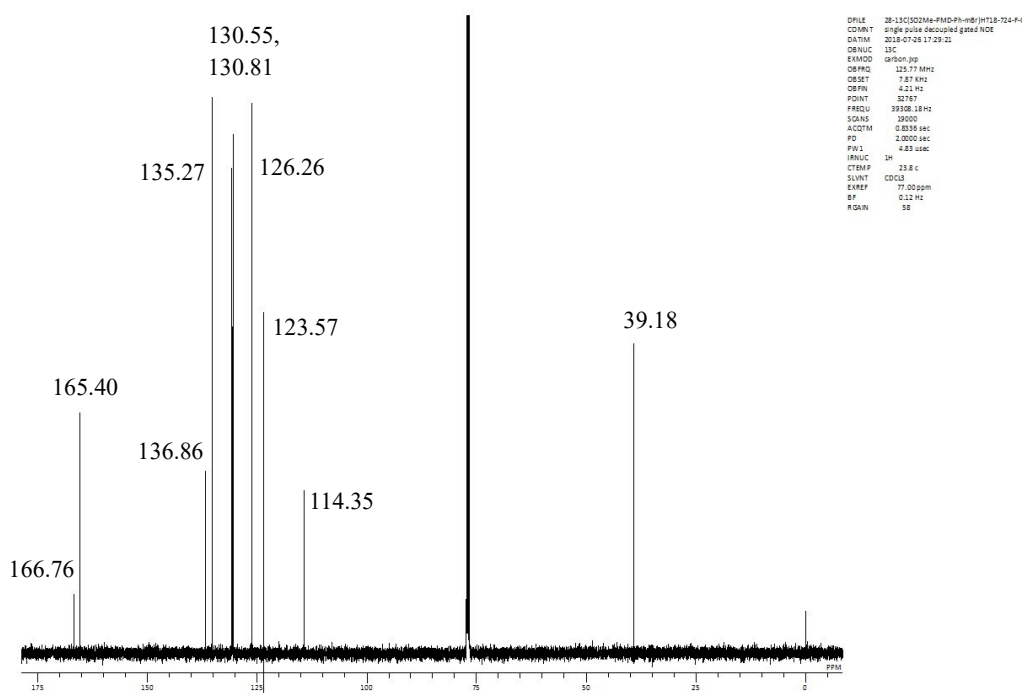
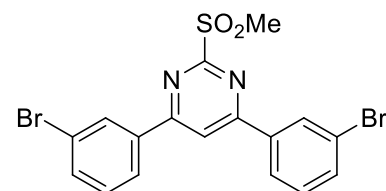


Fig. S50 ¹³C NMR spectrum of **7d** in CDCl₃.